

Heterogeneous Processes in the Atmosphere of Mars and Impact on H₂O₂ and O₃ Abundances



Key Points:

- Uptake of HO₂ on water ice on Mars could improve ozone simulations, but its unreliable support urges searches for alternative processes
- We introduce a range of new heterogeneous processes in a Mars general circulation model and evaluate their impact on ozone and H₂O₂
- We discuss the physical states of H₂O₂ on Mars, its photolytic destruction in ice, and the uptake of H₂O₂ and HO₂ by mineral dust

Supporting Information:

Supporting Information may be found in the online version of this article.

Correspondence to:









F. Daerden,
Frank.Daerden@aeronomie.be

Citation:

Daerden, F., Crowley, J. N., Neary, L., Smith, M. D., Loeffler, M. J., Clancy, R. T., et al. (2023). Heterogeneous processes in the atmosphere of Mars and impact on H₂O₂ and O₃ abundances. *Journal of Geophysical Research: Planets*, 128, e2023JE008014. <https://doi.org/10.1029/2023JE008014>

Received 19 JUL 2023

Accepted 6 NOV 2023

Frank Daerden¹ , John N. Crowley² , Lori Neary¹ , Michael D. Smith³ , Mark J. Loeffler⁴ , R. Todd Clancy⁵ , Michael J. Wolff⁵ , Shohei Aoki⁶ , and Hideo Sagawa⁷

¹Royal Belgian Institute for Space Aeronomy (BIRA-IASB), Brussels, Belgium, ²Max-Planck Institute for Chemistry, Mainz, Germany, ³NASA Goddard Space Flight Center, Greenbelt, MD, USA, ⁴Northern Arizona University, Flagstaff, AZ, USA, ⁵Space Science Institute, Boulder, CO, USA, ⁶Graduate School of Frontier Sciences, The University of Tokyo, Kashiwa, Japan, ⁷Faculty of Science, Kyoto Sangyo University, Kyoto, Japan

Abstract Current models underestimate the highest observed ozone (O₃) column densities on Mars. These estimates could be improved by including the uptake of odd hydrogen species (HO_x) on water ice clouds, but the reported uptake coefficient of HO₂ is likely overestimated for atmospheric conditions. This leaves a fundamental problem in Mars' atmospheric chemistry unsolved. Here, using the GEM-Mars general circulation model, we explore a range of processes involving multiple phases (gas, adsorbed and solid) that may contribute to an alternative solution. First, we focus on hydrogen peroxide (H₂O₂) and discuss its physical states on Mars and its chemical impact. We also conjecture its photolytic destruction in ices with model simulations and Compact Reconnaissance Imaging Spectrometer for Mars observations. Then, we include in the model all relevant (for Mars) heterogeneous reactions, both on dust and water ice, recommended by the International Union of Pure and Applied Chemistry for terrestrial atmospheric studies. We find that only the uptake of HO₂ and H₂O₂ on dust are efficient on Mars. Finally, we find that attenuation of sunlight by water ice clouds in the calculation of photolysis rates leads to increased O₃ and H₂O₂ abundances below the ice clouds. The combination of the proposed processes leads to O₃ increases without the need for strong uptake of HO₂ on ice, but it remains difficult to find a good agreement with O₃ and H₂O₂ observations on the global scale. We provide specific recommendations for future work in observations, laboratory experiments and modeling to advance our understanding of fundamental chemistry on Mars.

Plain Language Summary After decades of observations and numerical modeling, there remain persistent problems in our understanding of atmospheric chemistry on Mars. One of these is the underestimation of the highest ozone abundances by models, on which we focus here. It was demonstrated that uptake of HO₂ on water ice could improve this, but we argue that the experimentally obtained reaction rate is too large. We present a range of other processes that can contribute to solving the Mars ozone problem, and implement them in a 3D atmospheric model. We investigate the low temperature behavior of H₂O₂ on Mars and its impact on ozone, and demonstrate that H₂O₂ is destroyed in surface ices. This is supported by a first search for H₂O₂ in surface ices on Mars. We also test all heterogeneous reactions on dust and water ice that are recommended for the terrestrial atmosphere, and find that the uptake of HO₂ and H₂O₂ by mineral dust could be efficient on Mars. Finally, we find that the shielding of incoming sunlight by water ice clouds leads to larger ozone abundances below the clouds. Combining these processes improves the ozone simulation, but more refinements are still needed in observations, laboratory experiments and modeling.

1. Introduction

Ozone (O₃) is a highly reactive species in the Martian atmosphere, and one of the more commonly observed constituents (e.g., Clancy et al., 2016; Daerden, Neary, Wolff, et al., 2022; Khayat et al., 2021; Lebonnois et al., 2006; Lefèvre et al., 2021; Maättänen et al., 2022; Montmessin and Lefèvre, 2013; Montmessin et al., 2017; Olsen et al., 2020; Patel et al., 2021; Perrier et al., 2006; Piccialli et al., 2023; Willame et al., 2017). It has been known for several decades that odd hydrogen species (OH, HO₂, referred to as HO_x), that are formed after photolysis of water vapor, play key roles in Mars' atmospheric chemistry, and in controlling the abundances of ozone (McElroy and Donahue, 1972; Parkinson and Hunten, 1972; see Lefèvre and Krasnopolsky, 2017, for an overview). Atmospheric models of increasing complexity are able to reproduce the general patterns of seasonal and spatial ozone distributions (Clancy & Nair, 1996; Daerden et al., 2019; Daerden, Neary, Wolff, et al., 2022;

© 2023. The Authors.

This is an open access article under the terms of the [Creative Commons Attribution-NonCommercial-NoDerivs License](https://creativecommons.org/licenses/by-nc-nd/4.0/), which permits use and distribution in any medium, provided the original work is properly cited, the use is non-commercial and no modifications or adaptations are made.

Holmes et al., 2017, 2018; Krasnopolsky, 2006, 2009; Lefèvre et al., 2004, 2008, 2021; Moreau et al., 1991; Neary and Daerden, 2018). This led to increased confidence that the fundamental atmospheric chemistry of the Martian atmosphere is well understood.

However, there remain some persisting unsolved problems. To start with, odd hydrogen species have never been directly observed, leaving a crucial gap in our fundamental knowledge of Mars. Only in one case, airglow resulting from OH Meinel band emission was detected (Clancy et al., 2013). The situation is different for hydrogen peroxide (H_2O_2). This is a reservoir species for HO_x , that undergoes frequent exchanges with both OH and HO_2 , as such, it can be considered as a proxy to HO_x . It has a lifetime of several hours on the dayside. H_2O_2 has been detected on several occasions in the sub-millimeter and IR spectral ranges (Clancy et al., 2004; Encrenaz et al., 2004, 2012, 2015, 2019), and so is the only observed species directly connected to the odd hydrogen budget on Mars. Nevertheless, the available H_2O_2 data set is sparse, with eight detections and four non-detections (Clancy et al., 2004; Encrenaz et al., 2004, 2012, 2015, 2019; Hartogh et al., 2010; Krasnopolsky et al., 1997), and is highly variable, with a wide range of values observed in similar seasons during different Martian years.

Notoriously, even the very stability problem of the Martian CO_2 -rich atmosphere is still not fully understood. CO_2 is photolyzed into CO and O, but the recombination is spin-forbidden and so very slow. This implies that the CO_2 in the Martian atmosphere would have been largely decomposed into CO and O, but this is not the case. McElroy and Donahue (1972) and Parkinson and Hunten (1972) proposed two pathways that would lead to an efficient recombination of CO_2 through reactions with HO_x . 1D photochemical modeling for global-mean conditions is currently still the only tool to predict mean absolute abundances of long-living species on Mars (O_2 , CO, but also H_2). However, the CO abundances predicted by these models are smaller than those observed by a factor of ~ 5 (e.g., Lefèvre and Krasnopolsky, 2017). This indicates that there is a fundamental, not well understood problem with HO_x on Mars.

A related problem is the model underestimation of the largest observed ozone column abundances (Clancy et al., 2016; Daerden et al., 2019; Lefèvre et al., 2008, 2021), as ozone abundances are controlled by HO_x . These highest observed ozone columns are present in the polar regions, in particular in the north before and after the polar winter, and persistent during springtime, and in the south prior to the polar winter (e.g., Clancy et al., 2016). Model underestimation of ozone could be related to inaccurately simulated water vapor profiles, resulting in inaccurate HO_x vertical profiles. However, total ozone columns are in most cases dominated by the lowermost atmosphere and total water columns are well simulated in atmospheric models (e.g., Daerden et al., 2019; Lefèvre et al., 2021), so they should lead to a good ozone column simulation. It remains unclear why this is not the case.

It has been proposed that the model underestimation of ozone could be related to heterogeneous chemistry (Lefèvre et al., 2008). Heterogeneous processes impacting on atmospheric chemistry are well-known in the terrestrial atmosphere, for example, in relation to the formation of the Antarctic ozone hole (Solomon, 1999), but also for a much wider range of processes (George et al., 2015). Heterogeneous processes were also considered on Mars by several authors in 1D models (e.g., Anbar et al., 1993; Atreya & Gu, 1994; Brown et al., 2022; Krasnopolsky, 1993, 2006, 2009). After noticing a correlation of model-data ozone biases with the presence of water ice clouds, Lefèvre et al. (2008) implemented heterogeneous uptake of HO_x on water ice in a 3D general circulation model (GCM) using the uptake coefficients measured by Cooper and Abbatt (1996). In several parts of the ozone climatic cycle, this approach proved successful when compared to both MARCI (Clancy et al., 2016) and SPICAM (Lefèvre et al., 2008, 2021) O_3 column observations. This was in particular the case for north polar springtime conditions, and in the aphelion cloud belt (ACB). At high northern latitudes, also model $\text{H}_2\text{O}-\text{O}_3$ correlations could be improved compared to observations (Lefèvre et al., 2021). However, there was no clear improvement at the equator and at high southern latitudes, suggesting that the process considered did not uniquely solve the problem. Lefèvre et al. (2021) explored several photochemical parameters in the model to check for their impact on the $\text{H}_2\text{O}-\text{O}_3$ correlations, but found none with any significant impact.

The experimental result of Cooper and Abbatt (1996) for HO_2 uptake on ice was obtained for concentrations that far exceed those in the atmosphere. As a result, it is not recommended for atmospheric applications by the International Union for Pure and Applied Chemistry (IUPAC, Crowley et al., 2010). This poses a problem for Mars atmospheric chemistry models, as the current best solution for the ozone deficit problem would depend on a reaction with uncertain reliability or applicability. In this paper, we will use a Mars GCM to look for alternative solutions to the ozone deficit problem. As a start, we will more fully investigate the potential role H_2O_2 plays in controlling the ozone abundance on Mars. More specifically, we will test prior assumptions regarding what

happens to H_2O_2 when its concentration exceeds the saturation vapor pressure (Daerden et al., 2019; Lefèvre et al., 2004; Moudden, 2007). As part of this, we will propose a new type of adsorption isotherm of H_2O_2 on Martian water ice. We will also present the first effort to search for signatures of H_2O_2 in Mars surface ice using measurements taken by the Compact Reconnaissance Imaging Spectrometer for Mars (CRISM) spectrometer (Murchie et al., 2007) on Mars Reconnaissance Orbiter (Zurek and Smrekar, 2007).

In addition, we will implement all Mars-relevant heterogeneous reactions involving HO_x , O_x , and H_2O_2 , following the recommendations of IUPAC for atmospheric applications on Earth, and evaluate their impact on simulated chemistry by comparing to O_3 and H_2O_2 observations.

Finally, we will also revisit previous work (Daerden et al., 2019; Lindner, 1988) investigating how taking into account attenuation of sunlight by water ice clouds could alter the photolysis rates and the ozone abundances. This process could represent an alternative or complementary explanation for the correlation of the ozone deficit with water ice clouds.

While this paper may not provide a unique solution to the Mars ozone deficit problem nor to other fundamental problems regarding Mars chemistry, it intends to contribute to the understanding of the complexities in heterogeneous processes on Mars. As such, we aim to provide insights that guide future work in modeling, laboratory studies, ground-based observations, and in space missions.

2. Physical States of H_2O_2 on Mars

2.1. Introduction

Mars atmospheric chemistry was simulated in 3D GCMs by Lefèvre et al. (2004, 2008, 2021), Moudden and McConnell (2007), Holmes et al. (2017, 2018), Neary and Daerden (2018), Daerden et al. (2019), and Daerden, Neary, Wolff, et al. (2022). As noted above, HO_x species are highly reactive and are expected to control fundamental chemistry processes on Mars, but have never been observed. Hydrogen peroxide (H_2O_2) is a relatively stable reservoir species of HO_x , and far more abundant, which makes it also observable. Apart from CO_2 and H_2O , H_2O_2 is the only trace component that can reach saturation under Martian atmospheric conditions (Lindner, 1988). However, contrary to H_2O and CO_2 , it was never clearly understood how model studies should treat saturated H_2O_2 . In some previous model studies (Daerden et al., 2019; Moudden, 2007), saturated H_2O_2 was permanently removed from the atmosphere, while Lefèvre et al. (2004) follow the deposition/sublimation cycle of H_2O_2 throughout the atmosphere, but do not re-sublimate H_2O_2 deposits from the surface. These assumptions may have an impact on the chemistry simulations, and thus in this section we will explore the behavior of H_2O_2 at low, Martian atmospheric, temperatures.

2.2. Comparing the H_2O_2 and H_2O Phase Diagrams on Mars

Principally formed from the self-reaction of HO_2 , hydrogen peroxide (H_2O_2) is present both in the terrestrial and Martian atmospheres, in the latter as a by-product of water vapor photolysis. On Mars, H_2O_2 is photolyzed with a rate coefficient of, for example, $\sim 5 \times 10^{-5} \text{ s}^{-1}$ at 20 km, and so has a lifetime of ~ 6 hr in daylight (Daerden et al., 2019). Its IR and microwave absorption features make it uniquely observable among the fundamental photochemical minor species of the Martian atmosphere (Clancy et al., 2004; Encrenaz et al., 2019 and references therein). Its abundances have been found to be of the order of 10 parts per billion by volume (ppbv). The photochemical behavior of H_2O_2 has been discussed previously (e.g., Lefèvre and Krasnopolsky, 2017). Here we focus on the physical properties of H_2O_2 under Martian conditions, that is, low temperature (100–300 K) and pressure (<610 Pa).

Laboratory studies have shown that liquid mixtures of H_2O_2 and H_2O cause considerable freezing point depressions compared to pure H_2O , down to almost -60°C (213 K) for weight percentages of $\sim 50\%$ H_2O_2 (Foley & Giguere, 1951a). However, there was no freezing point depression for very low H_2O_2 concentrations, which are more relevant to any gas mixtures that would exist on Mars. For temperatures below the mixture's frost point, ices form that are either composed of pure H_2O ice and the H_2O_2 -dihydrate ($\text{H}_2\text{O}_2 \cdot 2\text{H}_2\text{O}$), or solid H_2O_2 and $\text{H}_2\text{O}_2 \cdot 2\text{H}_2\text{O}$ (Giguère, 1975).

Martian temperatures are mostly below the H_2O_2 triple point temperature (272.27 K), and so H_2O_2 in the gas-phase can saturate and deposit as a solid. The H_2O_2 abundances on Mars are too low to exceed the triple point vapor pressure of 34.66 Pa (Foley & Giguere, 1951b), and so liquid H_2O_2 cannot form. Lindner (1988) and

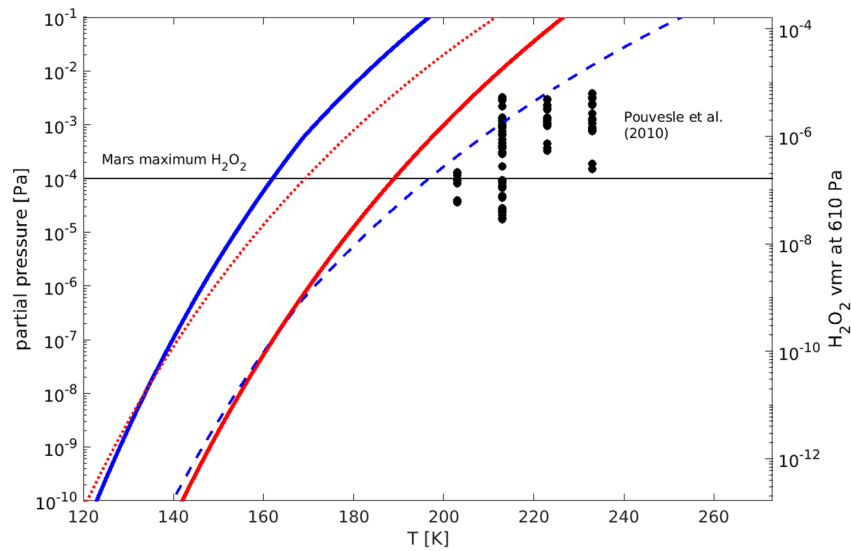


Figure 1. Phase diagram of H_2O (blue) and H_2O_2 (red) relevant for Martian conditions. The water saturation vapor pressure (blue, full) was taken from Marti and Mauersberger (1993) ($T > 169$ K) and Mauersberger and Krankowsky (2003) ($T < 169$ K). The H_2O_2 saturation vapor pressure over solid (red, full) was taken from Lindner (1988). The dashed blue line shows the water saturation vapor pressure scaled by 1,000. The red dotted line is the H_2O_2 saturation pressure over liquid, from Maass and Hiebert (1924), extrapolated to below the triple point. The right hand side axis shows H_2O_2 volume mixing ratio at 610 Pa, that is, the mean Mars surface pressure. The black symbols indicate the H_2O_2 vapor pressures and temperatures of the experiments of Pouvesle et al. (2010). The horizontal black line indicates the upper range of H_2O_2 values found in the GEM-Mars model (Daerden et al., 2019).

Krasnopolsky (1986) provided expressions to calculate the saturation vapor pressure and number density of H_2O_2 , respectively. The expression provided by Lindner (1988) is based on data provided in Kong and McElroy (1977). These authors provided a low-temperature extrapolation for the vapor pressure of H_2O_2 over its own solid using the Clausius-Clapeyron equation with the heat capacity data provided by Schumb et al. (1955) and solid H_2O_2 properties reported in Giguère et al. (1954). The expression by Krasnopolsky (1986) is based on a data fit between 140 and 190 K, with the data not specified, and the expression given in terms of number density. We verified that for specific combinations of pressure and temperature relevant for Mars, both expressions are similar. To the best of our knowledge, the vapor pressure of H_2O_2 over its own solid has never been measured (except at the triple point, G. M. Kavanagh (Ph.D. Thesis, Mass. Inst. Technol., 1948) as cited in Foley and Giguère (1951b), where it was found to be 34.66 Pa as mentioned above). Therefore, the theoretical extrapolation provided by Lindner (1988) is currently still the best estimate for the saturation vapor pressure of H_2O_2 over its solid at low temperature.

On Mars, the ratio of the abundances of H_2O and H_2O_2 is at most $\sim 1,000$ (e.g., Daerden et al., 2019, see also Section 3.2). In Figure 1, we show phase diagrams of H_2O_2 and H_2O , applying this scaling factor of 1,000 for H_2O . The purpose of this scaling is to more easily see where either of these species become saturated. The phase diagrams of H_2O and H_2O_2 are relatively similar, as their triple points are very close (273.15 vs. 272.27 K, and 611.66 vs. 34.66 Pa). As the enthalpy of sublimation for both species is different (46.6 kJ/mol for H_2O and 61 kJ/mol for H_2O_2 , Giguère, 1975), the vapor-solid coexistence lines have different slopes (this was already mentioned by Kong and McElroy, 1977). As a result, there is a temperature above which H_2O can be saturated with H_2O_2 sub-saturated, and below this temperature H_2O_2 can be saturated with H_2O sub-saturated. The value of this “crossover” temperature depends on the actual ratio of the H_2O_2 and H_2O abundances. This suggests a potentially complex interaction between H_2O_2 and H_2O at low temperatures, as for a given temperature range, one of the gaseous species may interact with the solid (ice) of the other species. The interaction of H_2O_2 vapor with water ice has been measured in the laboratory (Pouvesle et al., 2010) and will be discussed next.

2.3. Low Temperature Interaction Between H_2O_2 and Ice

Irreversible uptake of H_2O_2 on water ice was considered in 1D models for Mars by Krasnopolsky (2006, 2009). These works discussed the large uncertainty on the uptake coefficient (γ) at the time and found a best fit between

model and observations for $\gamma = 3 \times 10^{-4}$. The uptake of H_2O_2 on ice is now known to be reversible in nature, so that use of a time independent uptake coefficient is inappropriate, and will lead to larger model losses of gas-phase H_2O_2 .

Pouvesle et al. (2010) presented laboratory experiments of adsorption of H_2O_2 on water ice for terrestrial, upper tropospheric temperatures (203–233 K), which are also representative for the Martian atmosphere. The H_2O_2 partial pressures used in those experiments are shown in Figure 1, and are close to the most elevated H_2O_2 abundances on Mars. The experiments demonstrated the reversible adsorption/desorption of H_2O_2 , and via Langmuir-type analysis derived the saturation surface coverage of $N_{\text{max}} = 4 \times 10^{14}$ molecules/cm². In none of the experiments was full monolayer-coverage observed, though the N_{max} value obtained is similar to several other trace gases that reversibly adsorb via hydrogen bonding to ice surfaces (Crowley et al., 2010). The temperature-dependent Langmuir partition coefficient was found to be larger than derived in earlier work (Clegg & Abbatt, 2001) and entirely compatible with the trend in ice-surface affinity with the free-energy of condensation of a large selection of trace gases (Pouvesle et al., 2010). Evaluation panels (IUPAC, NASA) have adopted the Pouvesle et al. (2010) result to model the interaction of H_2O_2 with terrestrial ice surfaces (Burkholder et al., 2019; Crowley et al., 2010).

Complementing the limited number of experimental studies, Picaud and Jedlovszky (2014) provided theoretical Monte Carlo calculations of the interaction of H_2O_2 vapor with water ice surfaces, also for tropospheric conditions. While confirming the strong affinity of H_2O_2 for ice surfaces observed by Pouvesle et al. (2010), Picaud and Jedlovszky (2014) additionally predicted the formation of multiple H_2O_2 layers, with a stronger interaction between them than the H_2O_2 - H_2O bonds of the first surface layer. Even at low coverage, they found that new H-bonds were formed between the adsorbed H_2O_2 molecules (i.e., both lateral and inter-layer bonding) and not between H_2O_2 and adsorbent water molecules. Picaud and Jedlovszky (2014) suggest that for lower temperatures and pressures, the uptake of H_2O_2 on ice should be following a type II or even type III isotherm whereby the forces between adsorbent and adsorbate are smaller than between the adsorbates. There is no unique form for a type III isotherm, but Brunauer et al. (1940) pointed out that the BET theory (Brunauer et al., 1938) generic formalism describes type III adsorption.

Langmuir theory provides an expression for the amount of gas that is adsorbed at a surface and assumes that lateral interactions (i.e., adsorbate-adsorbate interactions) are negligible, even near monolayer coverage (N_{max}). For a gas phase concentration n_g (molecules/cm³) of H_2O_2 , the surface coverage (in molecules/cm²) is given by:

$$N = N_{\text{max}} \times \frac{K_{\text{Lang}} n_g}{K_{\text{Lang}} n_g + 1}$$

with $N_{\text{max}} = 4 \times 10^{14}$ molecules/cm², and $K_{\text{Lang}} = K_{\text{linC}}/N_{\text{max}}$, with the partition coefficient K_{linC} (in cm) derived by Pouvesle et al. (2010) as:

$$K_{\text{linC}} = 2.1 \times 10^{-5} \times \exp\left(\frac{3,800}{T}\right)$$

Langmuir analysis is expected to break-down before the surface coverage approaches N_{max} if lateral interactions are strong. Some evidence of this may be seen in the Pouvesle et al. (2010) isotherms in which no clear plateau-region (defining N_{max}) was observed and which may indicate the impact of lateral interactions at high surface coverage.

When Langmuir theory breaks down and especially in the case of multi-layer adsorption, other isotherms such as BET (Brunauer et al., 1938, 1940) have to be applied. Using BET, the surface coverage N (molecules/cm²) is given by:

$$\frac{p/p_s}{N(1 - p/p_s)} = \frac{c - 1}{N_{\text{max}}c} \left(\frac{p}{p_s}\right) + \frac{1}{N_{\text{max}}c}$$

where p is the partial pressure of H_2O_2 , p_s the saturation vapor pressure, and c the BET constant.

Pouvesle et al. (2010) also analyzed their data at 213 K using the BET isotherm, but did not find a deviation from the Langmuir isotherm, indicating that the H_2O_2 partial pressures were well below the saturation vapor pressure at each temperature. For this analysis, Pouvesle et al. (2010) used a value for H_2O_2 saturation vapor pressure at

Table 1
Comparison of the Experimental Conditions of Pouvesle et al. (2010) When Using the H₂O₂ Vapor Pressures Over the Liquid and Solid Phases

	203 K		213 K		223 K		233 K	
	Liquid	Solid	Liquid	Solid	Liquid	Solid	Liquid	Solid
p_s (Pa)	0.0310	0.0018	0.1196	0.0109	0.4087	0.0575	1.2568	0.2619
Max. $C_* = p/p_s$	0.0041	0.0727	0.0270	0.2956	0.0072	0.0514	0.0030	0.0146
BET parameter	74.021	4.7853	123.54	11.504	196.93	25.565	301.61	53.048

213 K of 1×10^{-3} Torr (0.13 Pa), which they derived from Antoine parameters for the liquid phase at higher temperatures. However, as those conditions are below the triple point (272.27 K, 34.66 Pa), the saturation vapor pressure over the solid phase (Lindner, 1988) should be used (Figure 1), which is about a factor 10 lower than the liquid phase value (Table 1).

Here, we reanalyze the Pouvesle et al. (2010) experimental results using a BET isotherm and the H₂O₂ saturation vapor pressure of Lindner (1988). A BET isotherm should still reproduce the experimental results of Pouvesle et al. (2010) at their respective temperatures and concentrations but additionally enable us to extrapolate their experimental results to Martian conditions.

To derive a BET isotherm, we produced synthetic data from the Langmuir isotherm given by Pouvesle et al. (2010) over temperatures of 183–273 K at 5 K intervals. We calculated the BET parameter at each temperature by applying standard BET analysis, that is, plotting the synthetic data versus $C_* = p/p_s$ and then applying a linear extrapolation to $C_* = 0$. We show the BET parameters obtained for the four temperature data points measured by Pouvesle et al. (2010) in Table 1. Next, we made a Van 't Hoff plot to fit the BET parameter versus inverse temperature (Figure S1a in Supporting Information S1). The fit was done for the five highest temperatures to avoid deviations at lower temperatures when the H₂O₂ frost point is approached, and where the synthetic data derived from the Langmuir isotherm may no longer be valid. We find the resulting T-dependent BET parameter to be:

$$c = 6.2253 \times 10^8 \exp(-3792.8/T)$$

In addition, we find a value of $N_{\max} = 4 \times 10^{14}$ molecules/cm² (Figure S1b in Supporting Information S1), which is consistent with Pouvesle et al. (2010).

We can now apply the derived BET value to generic Martian conditions (lower temperatures and concentrations), while still reproducing the Pouvesle et al. (2010) results (see Figure S2 in Supporting Information S1).

Figure 2a compares the BET isotherm to the Langmuir isotherm in an example for conditions covered by Pouvesle et al. (2010): gas-phase concentration $n_g = 2 \times 10^{11}$ cm⁻³, saturation vapor pressure $p_s = 6 \times 10^{-4}$ Pa, volume mixing ratio (VMR) = 5 ppmv, and surface area density (SAD) = 10^{-5} cm²/cm³. While the Langmuir isotherm allows no more than 2% adsorption of H₂O₂ near the frost point, this goes up to 100% for the BET isotherm. In this example, over 10 (and up to 100) layers are adsorbed near the frost point. Figure 2b makes the comparison for an example of conditions at the Martian surface: $n_g = 6 \times 10^9$ cm⁻³, pressure $p = 610$ Pa, $p_s = 1.5 \times 10^{-5}$ Pa, VMR = 25 ppbv, and SAD = 5×10^{-6} cm²/cm³. A complete removal of H₂O₂ from the gas phase is seen several degrees above the H₂O₂ frost point (when Langmuir theory removes only 10% of the H₂O₂) and results in a coverage of three monolayers. This demonstrates the strong impact of the proposed BET isotherm for lower temperatures.

2.4. Solid State of H₂O₂ Under Martian Conditions

At this time, nothing is known about the exact state of solid H₂O₂ under Martian conditions. H₂O₂ has been found in polar ice caps on Earth, at temperatures higher than on Mars and at concentrations of up to hundreds of ppbv relative to water ice (Lamarque et al., 2011; Neftel et al., 1984, 1986; Sigg & Neftel, 1988). As a comparison, on Mars, our reference simulations predict concentrations up to tens of ppmv (see Section 3.2), relative to water ice, or two orders larger than found on Earth. Observations of surface ices on the Jovian moon Europa (~130 K)

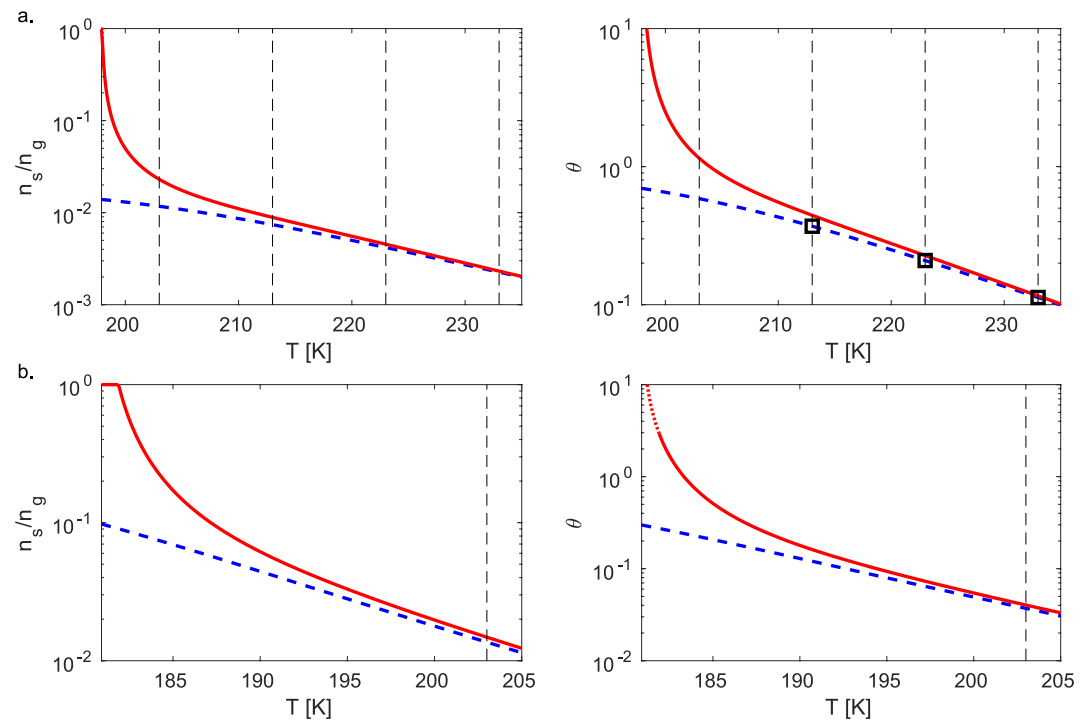


Figure 2. Examples of adsorption for (a) conditions given in Pouvesle et al. (2010), and (b) for Martian conditions (see text for details), for the Langmuir (blue) and BET (red) cases. The left plots show the fraction of uptake from the gas phase n_s/n_g , with $n_s (=SAD \times \theta \times N_{max})$ and n_g the number densities of adsorbed and gas phase H_2O_2 , respectively, and the right plots show the number of adsorbed layers (θ). The lower limit of the x -axis corresponds to the H_2O_2 frost point temperature in each case. The vertically dashed lines indicate the temperatures applied in Pouvesle et al. (2010). The black squares are the results of Pouvesle et al. (2010). In panel (b), the red dotted line shows the theoretical BET isotherm when all gas-phase H_2O_2 is adsorbed.

showed the presence of H_2O_2 at concentrations of $\sim 0.13\%$ (Carlson et al., 1999; Hand and Brown, 2013), similar to the higher ones in Martian ice caps predicted on Mars (see Section 3.2).

Previous laboratory experiments on solid solutions of H_2O_2 and H_2O can give some more basic insight into how these two compounds may interact in the Martian environment. Phase diagram experiments of mixtures of these two compounds show that there are three phases possible: pure H_2O , pure H_2O_2 , and $H_2O_2 \cdot 2H_2O$, and there are no more than two phases present at a time (Foley & Giguere, 1951a). Below the eutectic point, as on Mars, any mixture will be composed of pure H_2O and $H_2O_2 \cdot 2H_2O$ if the mixture has time to diffuse and reach equilibrium.

More recent laboratory experiments more analogous to an astronomical environment (Loeffler and Baragiola, 2005) show that the main conclusions from the older phase diagram studies regarding the phases present versus concentration are reasonable. These studies relied heavily on characterizing the sample using the $3.5 \mu m$ absorption band of H_2O_2 , whose shape and position are very sensitive to its environment. Here, we give more detail of the observed behavior in these laboratory experiments, attempting to place these results in context with the Martian environment.

Vapor deposition of a low concentration of H_2O_2 in H_2O at a low temperature (≤ 100 K) results in the $3.5 \mu m$ absorption band being broad and asymmetric, which was attributed to H_2O_2 being dispersed in the H_2O -ice (Loeffler and Baragiola, 2005). Warming these mixtures to ~ 130 K does not cause the $3.5 \mu m$ absorption band to change in shape or position, suggesting that it is energetically favorable for H_2O_2 to remain mixed in H_2O , rather than precipitate into pure aggregates.

This conclusion is supported by separate experiments where H_2O_2 and H_2O were vapor deposited in alternating layers at 110 K (Loeffler and Baragiola, 2005). After deposition, the $3.5 \mu m$ absorption band is symmetric and shifted to shorter wavelengths. However, annealing these mixtures at 125 K, the band becomes asymmetric and shifts to longer wavelengths, resembling that of H_2O_2 dispersed in H_2O -ice, suggesting that even at these

low temperatures these two compounds can interdiffuse and prefer to mix. Further heating of these mixtures to temperatures found on the Martian polar caps (~ 150 K), allows the sample to quickly crystallize into a mixture of crystalline H_2O and crystalline $\text{H}_2\text{O}_2 \cdot 2\text{H}_2\text{O}$. This crystalline mixture is also what was observed when the samples were vapor deposited at 150 K (Loeffler and Baragiola, 2011; Loeffler et al., 2006). Thus, we expect that anywhere we would find H_2O_2 and H_2O on the Martian surface, that the H_2O_2 would be mixed thoroughly with H_2O and likely be found as the dihydrate compound as well.

Considering that the Martian environment is dynamic and has partial pressures of H_2O_2 and H_2O in the atmosphere which were not modeled in the cited laboratory studies, it seems reasonable to consider whether one could potentially build up H_2O_2 to the extent that precipitates of H_2O_2 could form and remain on the surface. Simply using a thermal argument, at the temperatures of the Martian poles (~ 150 K), precipitation of pure H_2O_2 will not occur unless the atomic ratio of the two compounds exceeds that of the eutectic composition (i.e., 1:2 H_2O_2 : H_2O ratio). However, laboratory studies have shown that this can happen even with mixtures with low concentrations of H_2O_2 if the mixture is held at a temperature where H_2O is able to preferentially sublime compared with H_2O_2 (Loeffler and Baragiola, 2011; Loeffler et al., 2006). In fact, even at ~ 150 K a crystalline mixture of H_2O and crystalline $\text{H}_2\text{O}_2 \cdot 2\text{H}_2\text{O}$ will transition first to a pure crystalline $\text{H}_2\text{O}_2 \cdot 2\text{H}_2\text{O}$ mixture, then to a mixture of crystalline $\text{H}_2\text{O}_2 \cdot 2\text{H}_2\text{O}$ and H_2O_2 , and finally to pure H_2O_2 as H_2O preferentially sublimates under vacuum (Loeffler and Baragiola, 2011). Thus, if there are regions on the Martian surface that have preferentially lost H_2O , then it is possible that regions of pure H_2O_2 could exist.

The experiments and calculations regarding H_2O_2 described above provide some insight into possible ways that H_2O_2 could interact with an H_2O -ice surface under Martian conditions. However, it is currently unclear whether the different behaviors predicted are conflicting or if they indicate that H_2O_2 adsorbed on top of H_2O is physically different from H_2O and H_2O_2 being deposited in alternating layers. To explore the fate of adsorbed H_2O_2 in detail with numerical modeling, we would need measurements of saturation vapor pressures of H_2O_2 over for example, H_2O_2 - H_2O solids (e.g., dihydrates), or solid mixtures. Yet even the more basic measurements of the saturation vapor pressure of H_2O_2 over its own solid are lacking, and thus our estimates (Figure 1) largely rely on a theoretical calculation (Kong and McElroy, 1977; Lindner, 1988). Thus, for the present paper, we will simply deposit H_2O_2 into a “solid” tracer when saturated using the expression of Lindner (1988). We will also treat H_2O_2 and H_2O , and their solids, independent of each other (except for the case of H_2O_2 adsorption which can only occur with H_2O ice present).

3. Simulating H_2O_2 and O_3 in a Mars General Circulation Model

3.1. Simulations Set-Up

The GCM that we apply here is the Global Environmental Multiscale model for Mars (GEM-Mars), which is described in detail in Neary and Daerden (2018), Daerden et al. (2019), and Daerden, Neary, Villanueva et al. (2022). All GCM simulations presented in this paper are for the conditions of Mars year (MY) 35. The total dust columns in the model are constrained by the daily maps of Montabone et al. (2015, 2019) for the same MY (see Data Availability Statement for details). The model is spun-up for 10 MYs without chemistry (each time repeating the MY 35 conditions), followed by 2 MYs with chemistry. The output is taken from the second of these years. This time scale is sufficient for the fast chemistry reactions discussed in this paper.

The abundance and distribution of water vapor in our model is an important constraint for both the H_2O_2 and O_3 chemistry. The GEM-Mars model currently still has a simple ice cloud scheme, including saturation at 100% relative humidity and monodispersed ice particles, with radii that vary with latitude and altitude (Daerden, Neary, Villanueva, et al., 2022). The resulting seasonal and latitudinal distribution of the water vapor column abundance (Figure S3 in Supporting Information S1) does not perfectly match observations, but has similar general (latitudinal, seasonal) trends. Also, it is similar to other models that apply more sophisticated cloud schemes (e.g., Haberle et al., 2019; Navarro et al., 2014). As in Haberle et al. (2019), our water vapor columns are usually below the observations, with a bias of typically $\sim 20\%$. From such a “dry” simulation, we expect H_2O_2 abundances to be underestimated also by $\sim 20\%$, and so that ozone abundances will also be higher in our simulations compared to observations. However, as we will show, for ozone this is not the case. This is the ozone deficit problem for Mars.

3.2. Reference Simulation: With H_2O_2 Sublimation

We will present the results from a range of simulations that include specific combinations of known or newly proposed processes. The acronyms that are used to identify each simulation are given in Table 2. In this section,

Table 2
Acronyms Used for the Simulations (or Combinations of Them) Shown in the Paper

Reference simulations	
HPS	Hydrogen Peroxide Sublimation from its solid
HPR	Hydrogen Peroxide Removal when saturated
C&A	Uptake of OH and HO ₂ on water ice following Cooper and Abbatt (1996)
Adsorption simulations	
LAN	Langmuir type adsorption of H ₂ O ₂ on water ice
BET	BET type adsorption of H ₂ O ₂ on water ice
Heterogeneous, irreversible uptake reactions	
X/Dust	Irreversible uptake of species X on mineral dust
X/Ice	Irreversible uptake of species X on water ice
X/Y/10	Irreversible uptake of species X on substance Y (uptake coefficient divided by 10)
HET	Combination of all heterogeneous processes
New photolytic processes	
JLO	Apply photolytic (J) Loss of H ₂ O ₂ in solid and adsorbed states
ICA	Ice Cloud Attenuation of photolysis rates
Final simulation	
FINAL	(HPS + JLO) + HET(HO ₂ /Ice/10, H ₂ O ₂ /Dust/10)

we will present our results from a simulation aimed at being a reference for all the other simulations. This reference simulation (Hydrogen Peroxide Sublimation; HPS) applies pure homogenous chemistry, allows hydrogen peroxide to sublimate from its solid, and does not include adsorption. More specifically, we deposit H₂O₂ into a “(pure) H₂O₂ solid” tracer and a “(pure) H₂O₂ surface deposit”, and these can sublimate when they become sub-saturated with respect to the H₂O₂ vapor pressure. We assume H₂O₂ and H₂O do not interact and that atmospheric solid H₂O₂ is in the form of spherical particles with sedimentation velocities equal to those of water ice (Daerden, Neary, Villanueva, et al., 2022). On the surface, we assume H₂O₂ can only sublimate when there is no CO₂ ice present, as CO₂ ice forms and sublimates at lower temperatures than H₂O₂ and will likely cover any H₂O₂ deposits. We also assume the permanent water ice cap does not contain H₂O₂ (this assumption will be discussed further).

Figure 3 (left panels) shows the simulated zonal mean seasonal cycle of the H₂O₂ column densities in the gas phase and in the condensed phase in the atmosphere and on the surface. This seasonal cycle has similarities to the well-known water vapor cycle (e.g., Figure 11 in Daerden et al., 2019). However, these two molecules do not have the same sources, as the main source of atmospheric H₂O is the northern permanent polar cap, while photolysis of H₂O and subsequent reactions are the main source of atmospheric H₂O₂. Interestingly, both species have comparable sinks as both gases can deposit at comparable conditions for temperature and pressure (Section 2.2), and both species can be photolyzed (e.g., Daerden et al., 2019). Figure 3 (right panels) shows the corresponding simulated zonal mean column density ratio of H₂O₂/H₂O in the gas phase and in water ice deposits in the clouds and on the surface. In all regions, H₂O₂ is more than three orders of magnitude less abundant than H₂O.

One new result from this HPS simulation is that H₂O₂ is sublimated from the seasonal polar caps, causing peaks in its atmospheric abundance at $L_s \sim 90^\circ$ (north pole) and $L_s \sim 270^\circ$ (south pole). This is similar to the behavior of water vapor (e.g., Figure 11 in Daerden et al., 2019) and could potentially be observed with remote sensing observations.

Figure 4 shows the zonally averaged latitude-height cross-sections for the gas phase and solid phase H₂O₂ VMR at the cardinal seasons, found in the HPS simulation. The H₂O₂ distribution across the year follows a seasonal pattern that is driven by orbital variations, which affect insolation, differential heating, and global circulation. This is, again, also seen and well-known for water vapor (e.g., Figure 13 in Daerden et al., 2019, and Figure 4a in Daerden, Neary, Villanueva, et al., 2022). However, there are also some differences in the distributions caused by the differences in saturation and photolysis of both species. For instance, unlike H₂O, the H₂O₂ VMR distribution

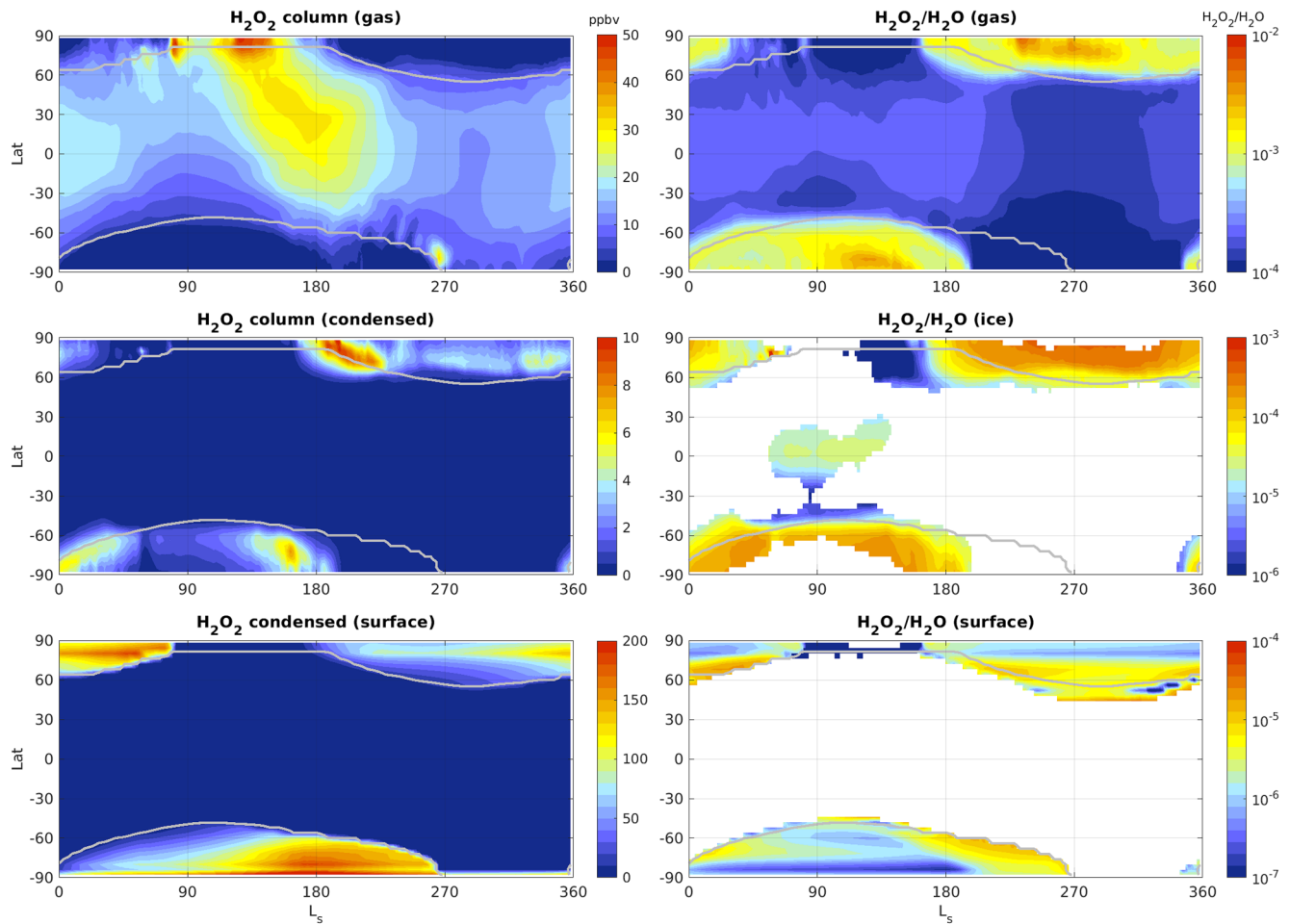


Figure 3. Zonally averaged results from the reference simulation (Hydrogen Peroxide Sublimation, see Table 2). (Left) H_2O_2 column in the gas-phase (top), and in the condensed phase in the atmosphere (middle) and on the surface (bottom). Total columns are relative to the air column. (Right) $\text{H}_2\text{O}_2/\text{H}_2\text{O}$ ratio in the gas phase (top), and in airborne ice (middle) and in surface ice (bottom). All fields were zonally averaged over all longitudes and local times. The gray contour lines represent the edges of the simulated seasonal and permanent polar ice caps. Note the differences in color scale for the various plots.

shows a maximum just below the main cloud level. This distribution is related to photolysis of H_2O , which acts as a source for H_2O_2 and has a rate increase with height from the surface up through the middle atmosphere (see Figure 1 in Daerden et al., 2019). Also, solid H_2O_2 can form outside of regions of H_2O ice cloud formation.

Figure S4 in Supporting Information S1 shows the average diurnal cycles of the H_2O_2 VMR at the cardinal seasons for selected latitudes. There are no large differences between the day- and nighttime H_2O_2 distribution, indicating this reservoir species is stable.

3.3. Resulting Ozone Simulation

Figures 5a and 5b show the zonally averaged daytime (local afternoon) ozone column derived from the HPS simulation, compared to the MARCI daytime (local afternoon) total ozone column observations (for MY 31; Clancy et al., 2016). We also show the ozone column calculated from a simulation of HO_x uptake on water ice using the Cooper and Abbatt (1996) uptake coefficients and assuming hydrogen peroxide removal upon saturation (HPR + C&A, Figure 5c). This HPR + C&A simulation is to certain degree equivalent to the “heterogeneous case” in Lefèvre et al. (2008, 2021), which however allowed for sublimation of H_2O_2 deposits in the atmosphere, but not for H_2O_2 deposits on the surface. (One more simulation is included in this figure but will be introduced in Section 8.)

The underestimation of the high latitude ozone columns is clearly visible in the HPS results, while the HPR + C&A case strongly improves the polar ozone deficit in the north. However, as was also found in Lefèvre et al. (2021), the improvement is less successful at high southern latitudes.

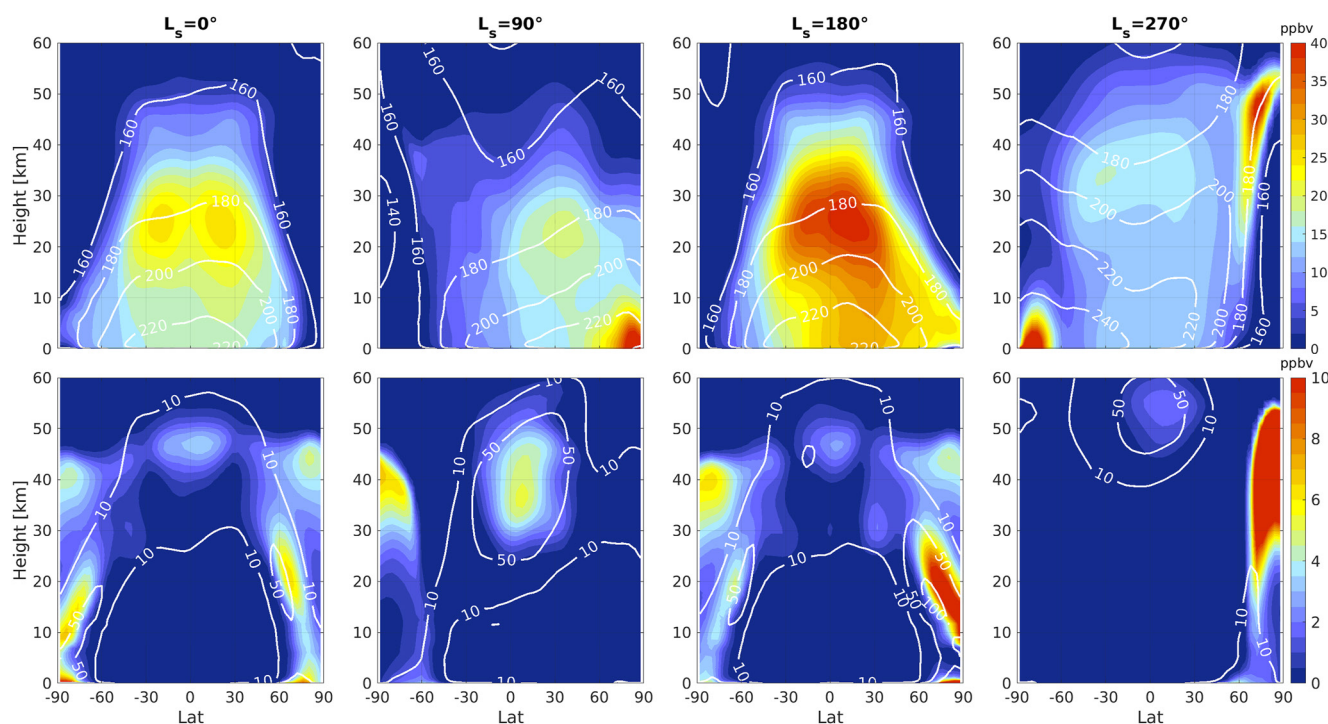


Figure 4. Latitude-height zonal mean vertical distribution of H_2O_2 in the gas phase (top) and in the solid phase (bottom) in the Hydrogen Peroxide Sublimation simulation, for the four cardinal seasons, averaged over all longitudes and local times and over 10 sols. White contour lines represent the temperature (top, in K) and the ice water content (bottom, in ppmv) as indication where water ice clouds form.

Figure 6 shows results for four different simulations (HPS, HPR, HPS + C&A, and HPR + C&A) of the O_3 columns averaged over three latitude bands of 30° width (90°S – 60°S , 15°S – 15°N , 60°N – 90°N), and of the dayside global averages of OH, HO_2 , and H_2O_2 , along with MARCI O_3 observations and the available H_2O_2 observations.

The HPS simulation predicts more H_2O_2 and less O_3 than do the other simulations. When solid H_2O_2 is forcibly removed (HPR), H_2O_2 abundances decrease and O_3 abundances increase. When the HPS simulation is combined with HO_x uptake (HPS + C&A), H_2O_2 abundances remain similar to the HPR results, but O_3 at northern springtime increases significantly. Finally, when HPR is combined with HO_x uptake (HPR + C&A), there is 20%–40% more O_3 present near the polar nights than in the HPS + C&A case, but there is no impact at northern springtime, when the columns still underestimate the MARCI data. Here, the O_3 columns in HPR and HPR + C&A cases are also below those of the respectively homogeneous and heterogeneous simulations in the LMD-GCM reported in Clancy et al. (2016), their Figure 11. Lefèvre et al. (2021) note that the water ice clouds in the version of Clancy et al. (2016) were too thick and that the heterogeneous chemistry impact was too strong. From a comparison of the GEM-Mars model with the Mars Climate Database (MCD) v6.1, it is found that in early springtime at high northern latitudes, GEM-Mars has more water vapor and less water ice clouds than MCD (see Figure S5 in Supporting Information S1), explaining why O_3 columns in GEM-Mars are below those in MCD in both cases.

Nevertheless, these results show that removal of H_2O_2 from the condensed phase has a positive effect on the simulated O_3 , but there is no clear physical reason for such removal. We will explore this more in Section 5.

4. Simulating H_2O_2 Adsorption on Water Ice

Here we implement the reversible adsorption of H_2O_2 on water ice (Section 2.3) in the simulations. To do this, we performed two different simulations: one using the Langmuir isotherm of Pouvesle et al. (2010) and one using the BET isotherm proposed in Section 2.3. The basic approach in these simulations is the HPS case, that is, solid H_2O_2 can sublimate. At every time step and grid point, we first check if H_2O_2 is saturated, and if this is the case it is deposited into the solid H_2O_2 tracer and no adsorption is considered. Next, we calculate the isotherm

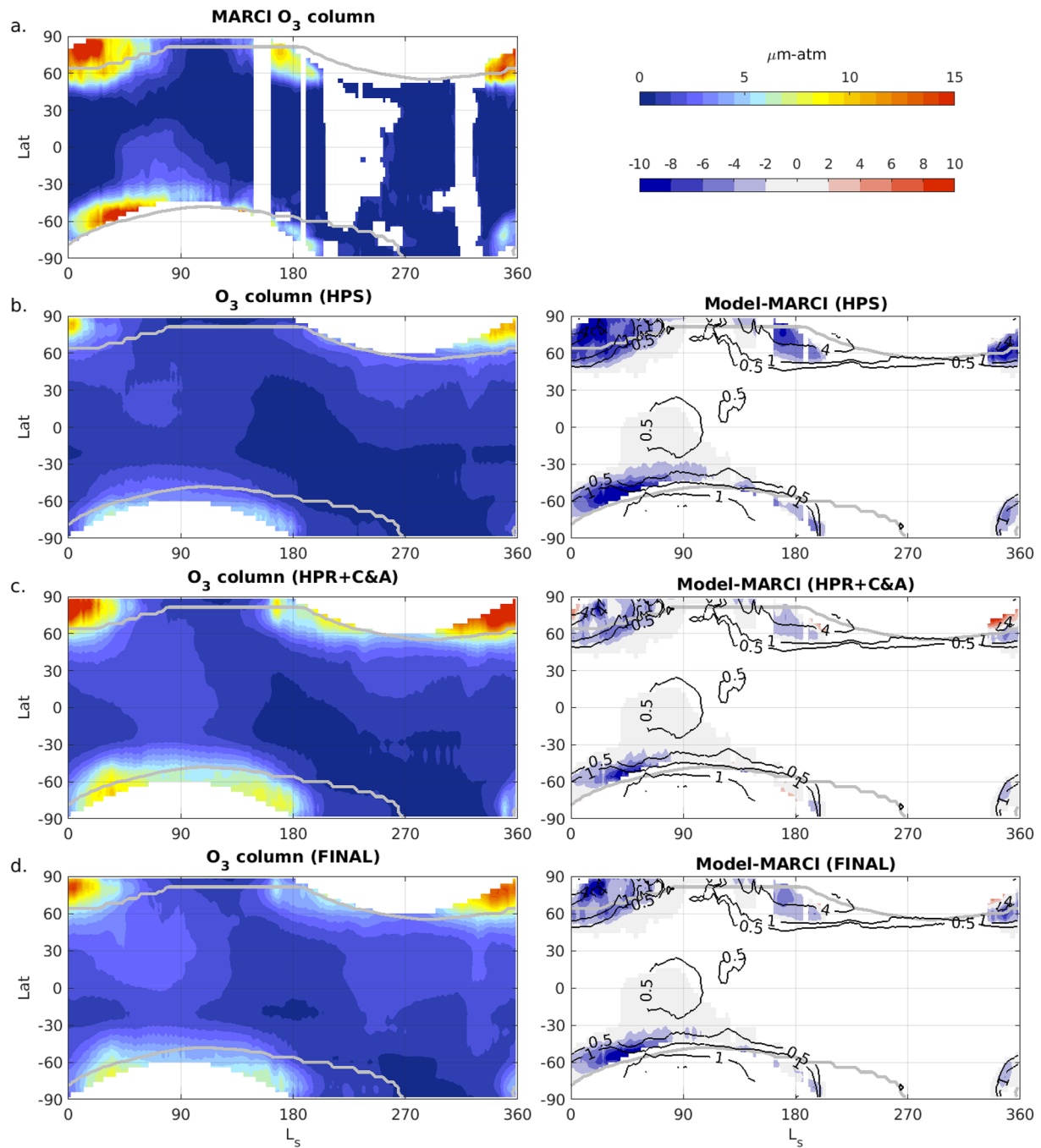


Figure 5. Zonal mean daytime (local afternoon) O_3 column from: (a) MARCI observations (Mars year 31; Clancy et al., 2016), (b) Hydrogen Peroxide Sublimation simulation, (c) HPR + C&A simulation, (d) FINAL simulation (without strong uptake of HO_x on ice, see Section 8). All results were averaged over 4° latitude and $2^\circ L_s$. The gray contour lines represent the edges of the simulated seasonal and permanent polar ice caps. The right column shows the difference between model and MARCI. Here, data was removed when MARCI O_3 was less than $1 \mu\text{m-atm}$ (the lower sensitivity limit). Black contour lines show the simulated daytime cloud Ice Water Content ($\text{pr-}\mu\text{m}$).

θ , which is based on the H_2O_2 concentration in the gas phase, and provides the concentration of the adsorbate, $n_s = \text{SAD} \times \theta \times N_{\text{max}}$ (see Section 2.3), where SAD is the SAD of ice. The adsorbed H_2O_2 is stored in an “ H_2O_2 adsorbate” tracer. We then update the number densities accordingly so that we reach this surface concentration, which can result in adsorption or desorption. We also assume that H_2O can sublimate independently from adsorbed or solid H_2O_2 , which is based on the experimental insights explained in Section 2.4.

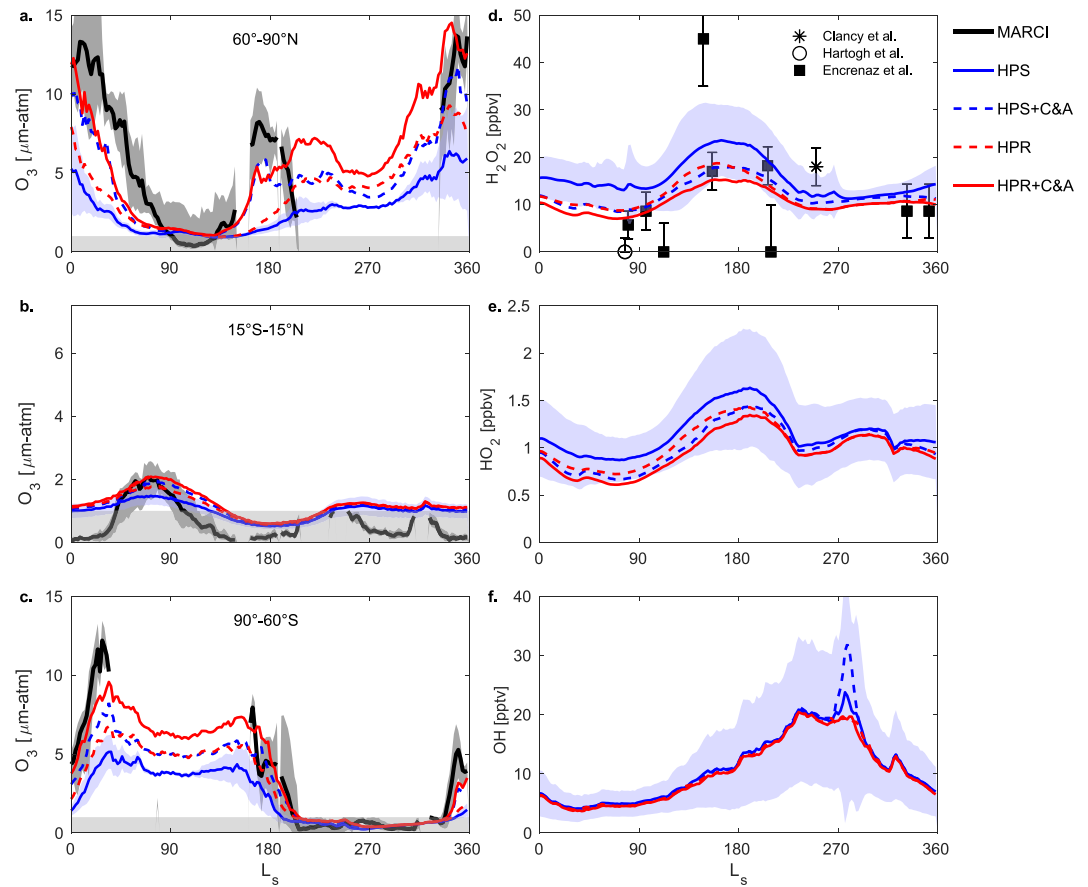


Figure 6. Comparison of model simulations for O_3 (a–c), H_2O_2 (d), HO_2 (e) and OH (f). For O_3 , model results are dayside, local afternoon (2–4 p.m., $SZA < 90^\circ$) columns, averaged over three 30° wide latitude bands as indicated. For H_2O_2 and HO_2 , model results are globally averaged dayside columns relative to air. Observations (black) are also shown for O_3 and H_2O_2 . MARCI O_3 observations (Clancy et al., 2016) are for approximately 3 p.m. and emission angles $< 70^\circ$ (explaining why there are none near the polar nights), and were averaged over the same latitude bands. H_2O_2 observations (Clancy et al., 2004; Encrenaz et al., 2019; Hartogh et al., 2010) were integrated over specific parts of the disk not always representative of the global dayside. All model output and O_3 observations were also averaged over 2° wide L_s bins. The dark gray shading represents the full range of MARCI O_3 columns within the latitude bands and L_s bins, and the light gray (horizontal) shading indicates $1 \mu\text{m-atm}$ which is the lower limit of sensitivity of MARCI retrievals. The blue shading represents the variability (1σ) of the Hydrogen Peroxide Sublimation simulation within the bands and bins.

Each model time step is ~ 30 min, which is long enough for the system to reach equilibrium. We estimated this by considering the uptake coefficient as a function of time, $\gamma(t) \sim e^{-Bt}$ (Crowley et al., 2010) with $B = \alpha_s \bar{c} n_g / 4N_{\text{max}} + k_{\text{des}}$, where α_s is the surface accommodation coefficient, \bar{c} the thermal velocity (cm/s), n_g the gas phase concentration (cm^{-3}), N_{max} as in Section 2.3, and k_{des} the desorption rate constant (s^{-1}). For high coverages, the first term in B dominates. For H_2O_2 on Mars, $\bar{c} \sim 3 \times 10^4$ cm/s, $n_g < 10^{11}$ cm^{-3} , and so (taking $\alpha_s = 1$) we estimate $B < 2$, which implies that the time scale to reach equilibrium is typically less than a second. For low coverages, k_{des} could dominate, with $k_{\text{des}} = \alpha_s \bar{c} / 4K_{\text{LinC}}$, and K_{LinC} (cm) as in Section 2.3. K_{LinC} increases with decreasing temperature and at a typical Martian temperature (150 K), $K_{\text{LinC}} \sim 2 \times 10^6$ cm, which yields $k_{\text{des}} \sim 0.003$ and implies the time scale to reach equilibrium is ~ 5 min, well below the model time step.

Adsorption can occur on all water ice surfaces, including water ice particles in the atmosphere as well as on the surface if it is covered with water ice (and not covered with CO_2 ice). The SADs of water ice in the model are discussed in Text S1, and shown in Figures S6, S8, and S9 in Supporting Information S1.

Figure 7 shows the simulated column densities of the adsorbed and solid H_2O_2 in the atmosphere and on the surface, for the simulations with Langmuir type adsorption and BET type adsorption. Compared to the Langmuir case, the BET results show a larger fraction of H_2O_2 in the adsorbed state, but less in the solid state. However, the

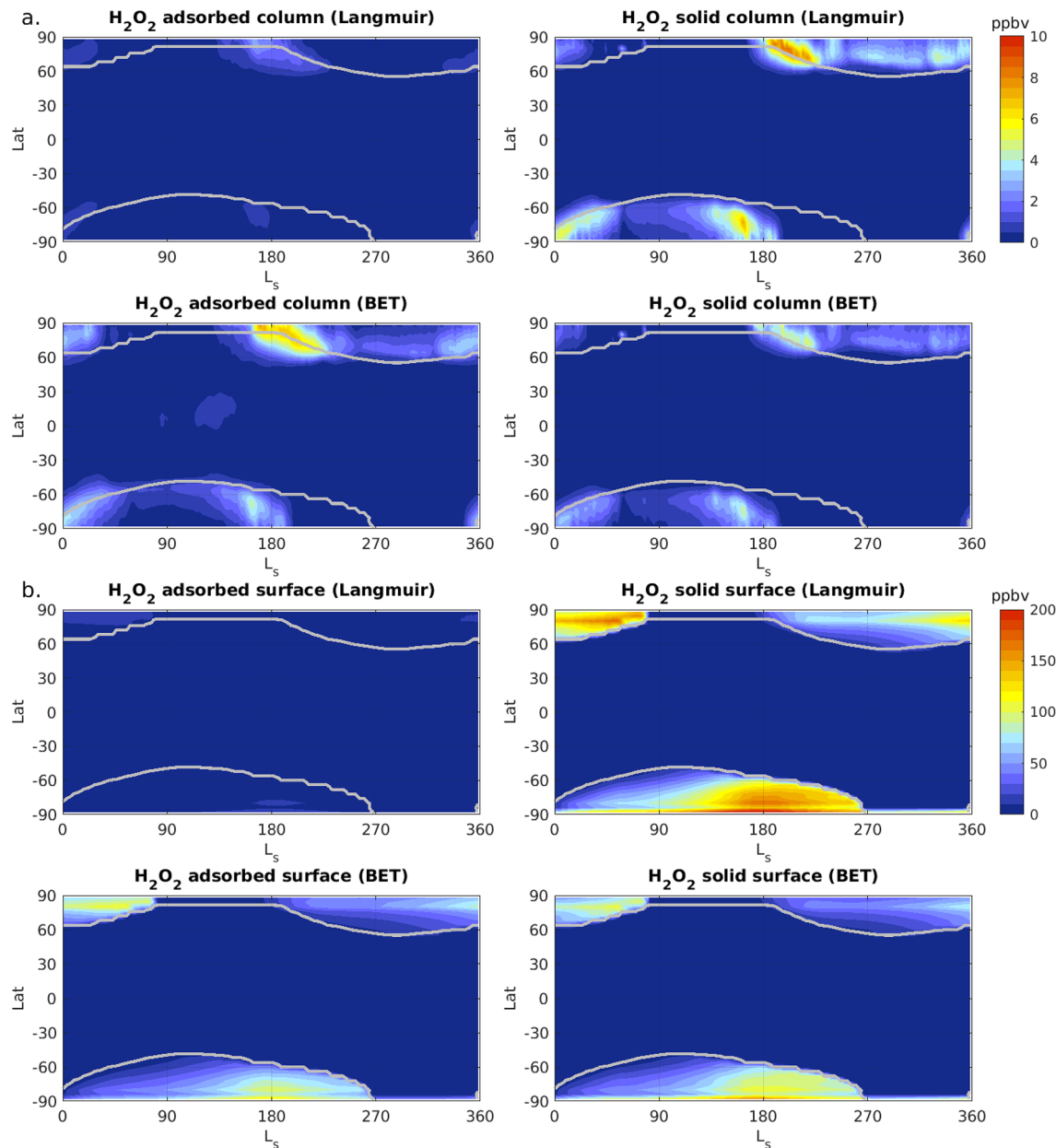


Figure 7. Zonally averaged H_2O_2 column in the adsorbed (left) and solid (right) state, in the atmosphere (a) and on the surface (b), from the simulations with Langmuir respectively BET adsorption (HPS + LAN, HPS + BET, see Table 2). Total columns are relative to the air column. All fields were zonally averaged over all longitudes and local times. The gray contour lines represent the edges of the simulated seasonal and permanent polar ice caps.

total amount of H_2O_2 removed from the gas-phase is comparable in both cases, and also comparable to the pure HPS case (Figure 3), suggesting that adsorption only repartitions H_2O_2 between the adsorbed and solid states throughout the atmosphere and on the surface. As a result, the overall impact on H_2O_2 abundances and on the resulting O_3 columns is very small (see Figure S10 in Supporting Information S1).

Figures 8 and 9 show the vertical distributions of adsorbed and solid H_2O_2 derived in these simulations. Also shown is θ , that is, the surface coverage of H_2O_2 adsorbed on water ice particles in fractions of N_{max} (see Section 2.3). θ is typically predicted to be one order of magnitude larger assuming BET adsorption compared to Langmuir adsorption. However, in both cases we find that the impact on gas-phase H_2O_2 is very small as the total amount of H_2O_2 removed from the gas-phase is similar for both simulations, and similar to the pure HPS case (Figure 4). These results are not too surprising, as the differences seen in adsorption occur in a temperature range

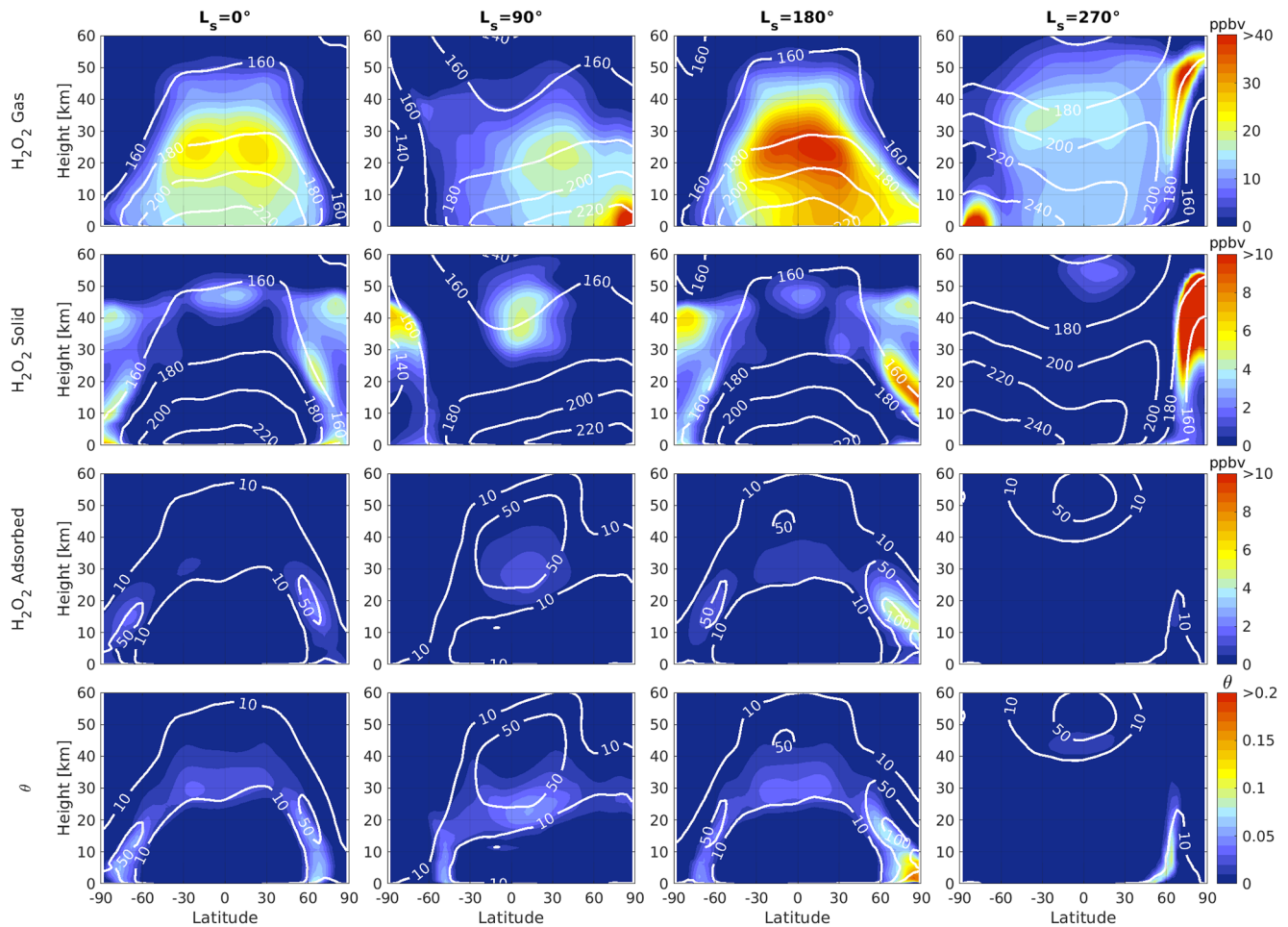


Figure 8. Latitude-height zonal mean vertical distribution of H_2O_2 in the gas (top), solid (second row), and adsorbed state (third row) in the Hydrogen Peroxide Sublimation (HPS) simulation including Langmuir type adsorption (HPS + LAN), for the four cardinal seasons, averaged over all longitudes and local times and over 10 sols. The bottom plots show the surface coverage (θ) as fraction of the monolayer coverage N_{max} (see text). White contours represent temperature (top, in K) and ice water content (middle and bottom, in ppmv) as indication where water ice clouds form.

of a few K above the H_2O_2 frost point (see Figure 2). However, once the temperature drops below the frost point, the same amounts are removed from the gas-phase in both cases, making the overall impact on H_2O_2 abundances and on resulting O_3 columns very small.

We conclude that adsorption of H_2O_2 on water ice on Mars likely happens, but the process is too weak to impact significantly O_3 abundances on a global scale. This is consistent with the 3D modeling work of Lefèvre et al. (2021) and the 1D modeling study of Brown et al. (2022), who both assumed Langmuir adsorption. Here we showed, using a 3D model, that the O_3 deficit problem cannot be solved even if we assume the stronger BET-type adsorption.

5. Photochemical Loss of H_2O_2 in the Condensed Phase

5.1. Photolytic Destruction of H_2O_2 in Condensed Phase

Loeffler et al. (2013) studied the photolytic destruction of H_2O_2 in H_2O - H_2O_2 ice mixtures between 21 and 145 K. They estimated that in most environments the photolytic destruction would be much higher than the H_2O_2 production rate from energetic particles, which could explain why H_2O_2 has rarely been detected in the solid phase.

Using the HPS simulation, we investigated the most likely source of H_2O_2 in the Martian seasonal polar caps (Figure 10, left). When keeping track of the source of the condensed H_2O_2 , we found that between direct deposition

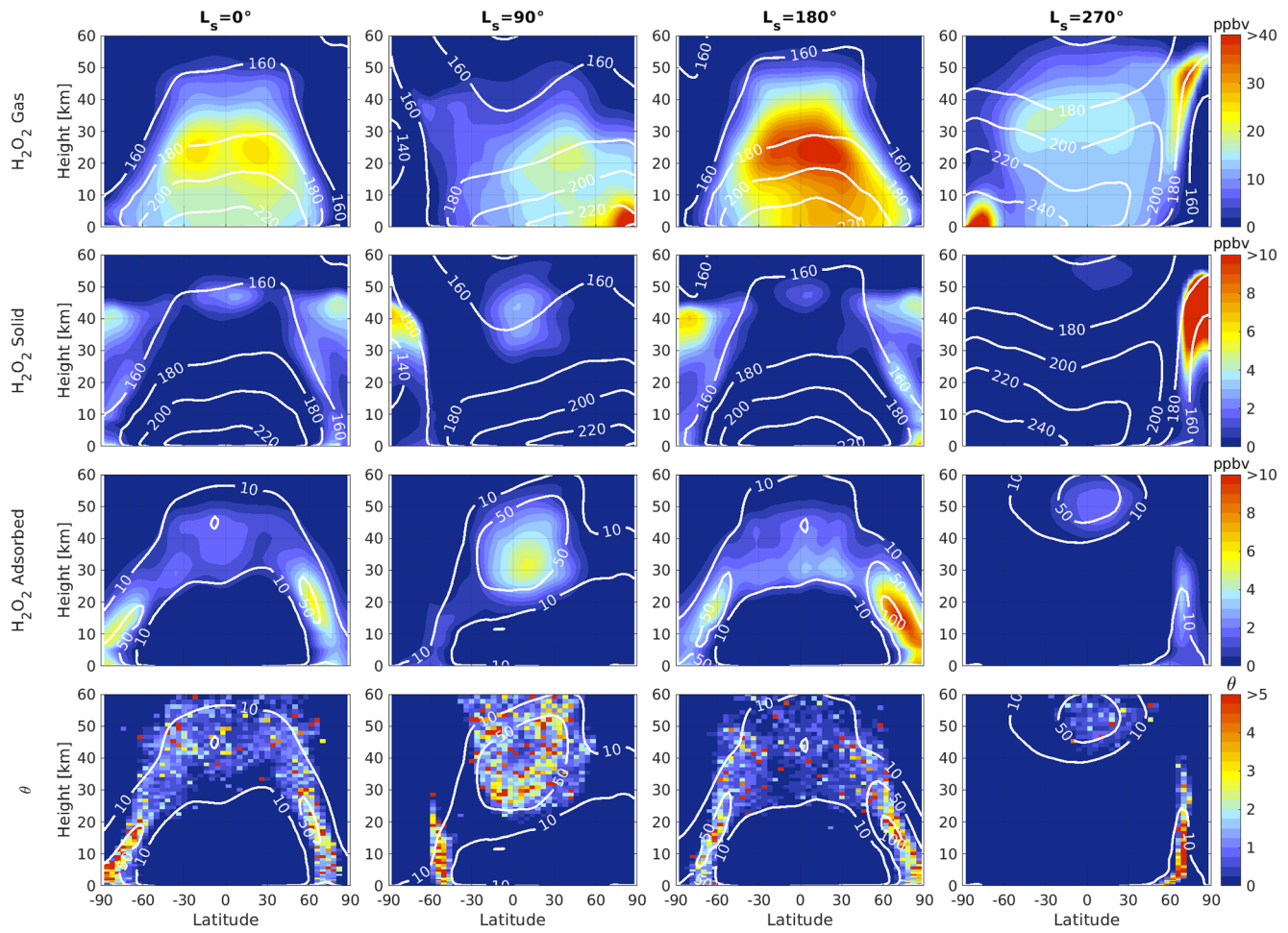


Figure 9. As Figure 8 but for the simulation using BET type adsorption (HPS + BET). Note the difference in color scale for θ (bottom plots) compared to Figure 8. The plots for θ were not smoothed as there are many localized high values (up to tens and in rare occasions even hundreds).

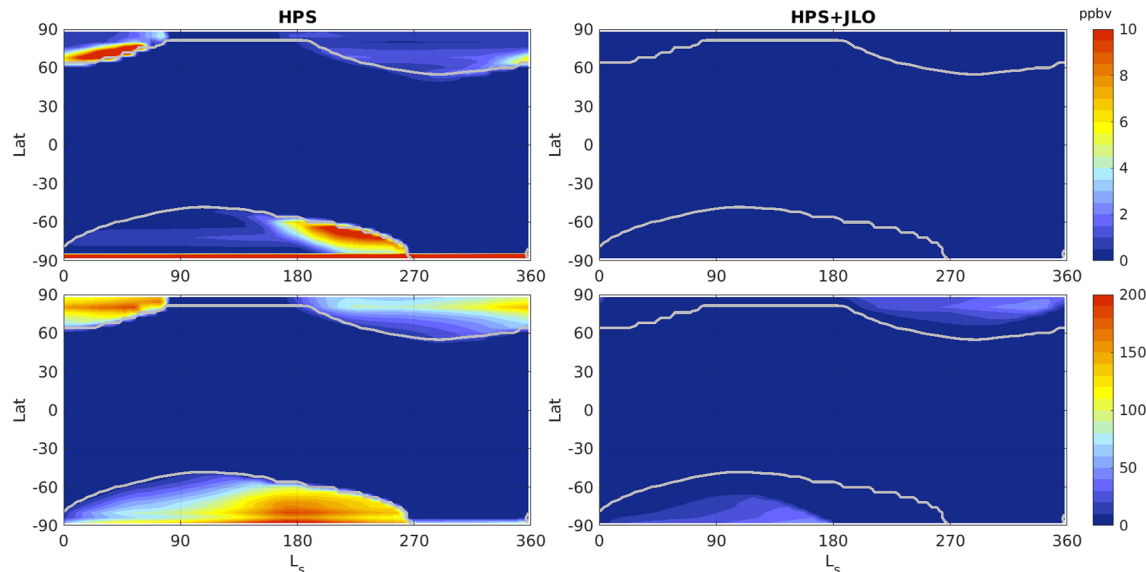
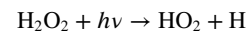
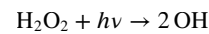


Figure 10. H_2O_2 surface deposits from either direct deposition (top) or from accumulated precipitation (bottom), for the Hydrogen Peroxide Sublimation (HPS) simulation (left) and the corresponding simulation with photolytic loss of H_2O_2 in solid deposits (HPS + JLO, right).

from the gas phase onto the surface, or precipitation of condensed H_2O_2 particles formed in the atmosphere, atmospheric precipitation is by far the dominant source. Considering that H_2O_2 in solid particles aloft in the atmosphere can be subject to solar UV radiation at higher altitudes and/or before they enter into the polar night, photolytic loss in airborne deposits should be considered in addition to direct photolytic loss in surface deposits.

We performed a simulation (HPS + JLO) including the photolytic loss of H_2O_2 in the condensed phase, both aloft and on the surface, using the same loss rates as those for atmospheric H_2O_2 following these reactions (see Daerden et al., 2019; Daerden, Neary, Wolff, et al., 2022):



of which the former is by far the dominant one, with photolysis rate ~ 2 orders of magnitude larger than the latter one (e.g., Daerden et al., 2019).

Figure 10 (right) shows the H_2O_2 on the surface after taking into account UV photolysis. For both sources of surface H_2O_2 , the amount of H_2O_2 on the surface is strongly reduced, by as much as an order of a magnitude, compared to the HPS simulation. For the deposits that come from precipitation, only some H_2O_2 (at most 20% relative to the HPS simulation) survives in the deposits, and only deep inside the polar night.

We conclude that the photolytic loss of H_2O_2 in the solid state is an efficient mechanism to remove H_2O_2 from deposits, a process which was previously included in models without a physical basis.

A consequence of this process is that there is likely no significant presence of H_2O_2 in at least the upper layers of the permanent water ice cap, which is fully exposed to sunlight when it becomes free of CO_2 ice in northern summer. By doing dedicated simulations in which we included initial presence of H_2O_2 in the permanent cap, as well as the photolytic destruction in the ice, we confirmed that any H_2O_2 in the cap would be quickly destroyed (not shown). As such, our assumption to not include H_2O_2 in the permanent cap (see Section 3.2) is valid.

Figure 11 shows how the HPS + JLO simulation affects the atmospheric H_2O_2 and O_3 columns. In general, taking into account photolytic loss of solid H_2O_2 moderately moves the calculated HO_x , H_2O_2 , and O_3 columns into the direction of the simulations with (forced) full solid state H_2O_2 removal (HPR).

The impact of the photolytic destruction may be stronger than considered here, as we should take into account further reactions in the ice. For instance, if the main products are two OH radicals, these will likely react further with H_2O_2 in the ice. As a result, depending on the H_2O_2 concentration, up to three H_2O_2 molecules could be lost per photon absorbed. Some H_2O_2 will be reformed though from self-reaction of HO_2 , unless HO_2 is depleted by reacting with something on the ice surface, for example, with OH to form H_2O and O_2 . This could be explored in future studies.

5.2. Observational Evidence for the Destruction of H_2O_2

Carlson et al. (1999) provide remote sensing spectra in the UV and IR corresponding to the presence of H_2O_2 in surface ices on the Jovian moon Europa, while Hand and Brown (2013) provide additional spectra in the IR region. Recently, Trumbo et al. (2023) reported the detection of H_2O_2 in the polar caps of the Jovian moon Ganymede. The IR feature, centered at 3,500 nm, should also be observable in spectra of Mars if H_2O_2 were present in Martian surface ices. We used spectra returned from the CRISM instrument (Murchie et al., 2007) on-board the Mars Reconnaissance Orbiter to search for the presence of H_2O_2 in Martian surface ices.

Figure 12 shows the seasonal and latitudinal distribution of CRISM observations in the northern hemisphere during the first half of the Martian year, containing the spectral signatures of surface H_2O ice, with blue points indicating ice-covered surfaces and red points indicating ice-free surfaces. This can be compared against Figure 10, which shows the possible locations of H_2O_2 surface deposits given by the simulations. Based on the observed spectral signature of H_2O_2 ice shown by Hand and Brown (2013) and by Carlson et al. (1999), we constructed a “3,500 nm index,” computed as $(I/F(3,400\text{ nm}) - 2 \times I/F(3,500\text{ nm}) + I/F(3,600\text{ nm}))$, with I the radiance observed by CRISM, F the solar radiance at the top of the Mars atmosphere, and I/F the normalized radiance. We then computed this index for all CRISM spectra taken over surface H_2O ice (those indicated by the blue points in Figure 12) to identify the spectra containing high 3,500 nm index, which would indicate the possible presence of H_2O_2 in the surface ice.

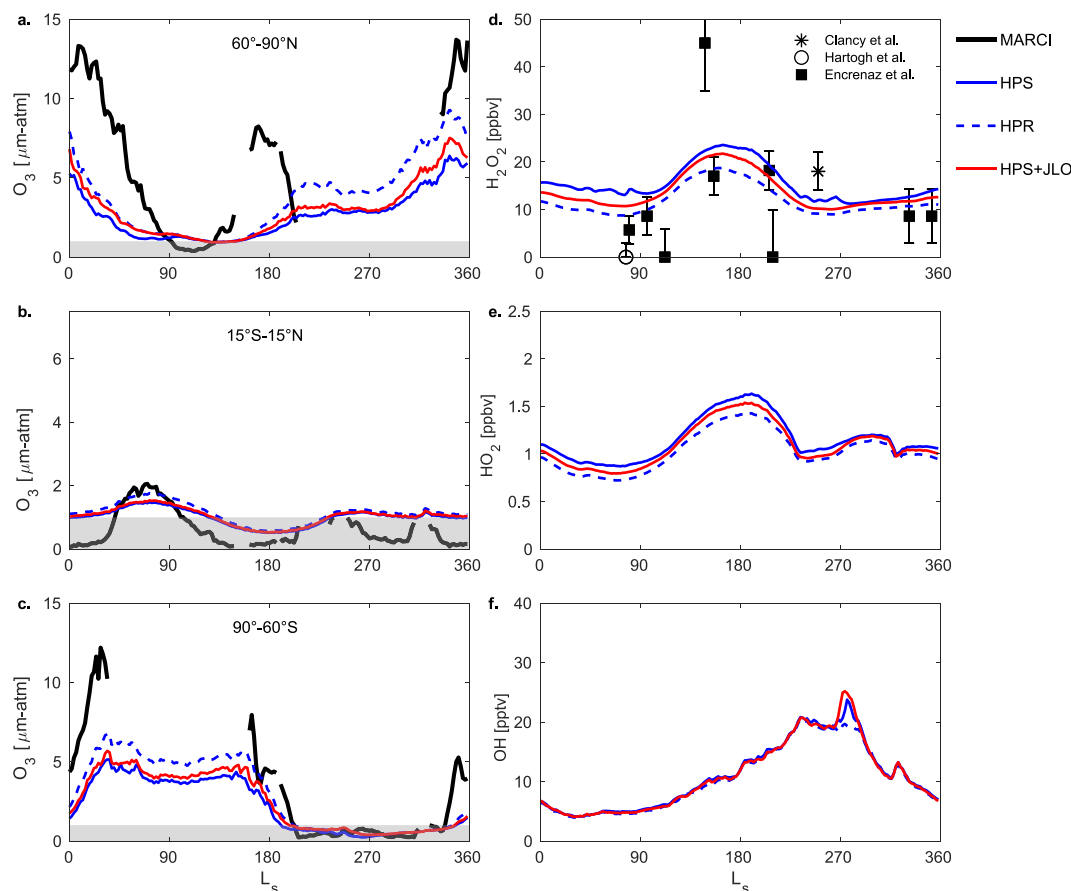


Figure 11. As Figure 6 but showing the simulation with photolytic loss of H_2O_2 in the condensed state (JLO, red lines) compared to the corresponding simulation without photolytic loss (blue full lines), and to the simulation with forced removal of H_2O_2 (blue dashed lines).

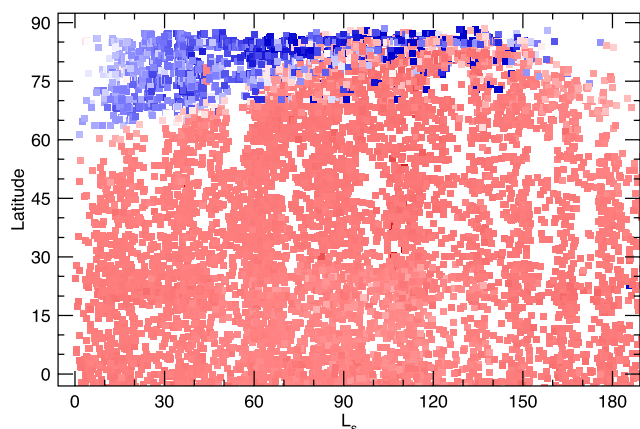


Figure 12. The seasonal and latitudinal distribution of Compact Reconnaissance Imaging Spectrometer for Mars observations of Mars showing the presence (blue points) or absence (red points) of the spectral signature of H_2O surface ice. We use those spectra indicating H_2O surface ice (the blue points) in our search for H_2O_2 .

Figure 13 shows the result of that search. The left two panels show observed CRISM spectra with relatively high 3,500 nm index (upper left panel; red spectra) and with relatively low 3,500 nm index (lower left panel; blue spectra). The differences between the two sets of spectra are relatively modest, but can still be identified by the consistent break in spectral slope at 3,500 nm in the spectra with high 3,500 nm index (red spectra in Figure 13). The upper right panel of Figure 13 allows a direct comparison by showing the averages of all of the “high 3,500 nm index” and of all the “low 3,500 nm index” spectra. The lower right panel of Figure 13 shows the ratio between the two averaged spectra. It is apparent that although there is a real spectral difference between the “high” and the “low” index spectra, that spectral difference does not correspond to the relatively narrow spectral feature of H_2O_2 . Instead, this spectral difference corresponds to that of H_2O ice clouds, which are well known to occur at this season and latitude on Mars (e.g., Khayat et al., 2023; Wolff et al., 2019).

This analysis of the CRISM spectra is currently purely qualitative. There is no detectable spectral signature of H_2O_2 in surface ice in the CRISM spectra, but we have not yet compared our results to simulated spectra of H_2O_2 in ice for a range of $\text{H}_2\text{O}_2/\text{H}_2\text{O}$ mixtures (see Figure 3). Therefore, we are currently unable to obtain an upper limit to this non-detection. This is envisaged in

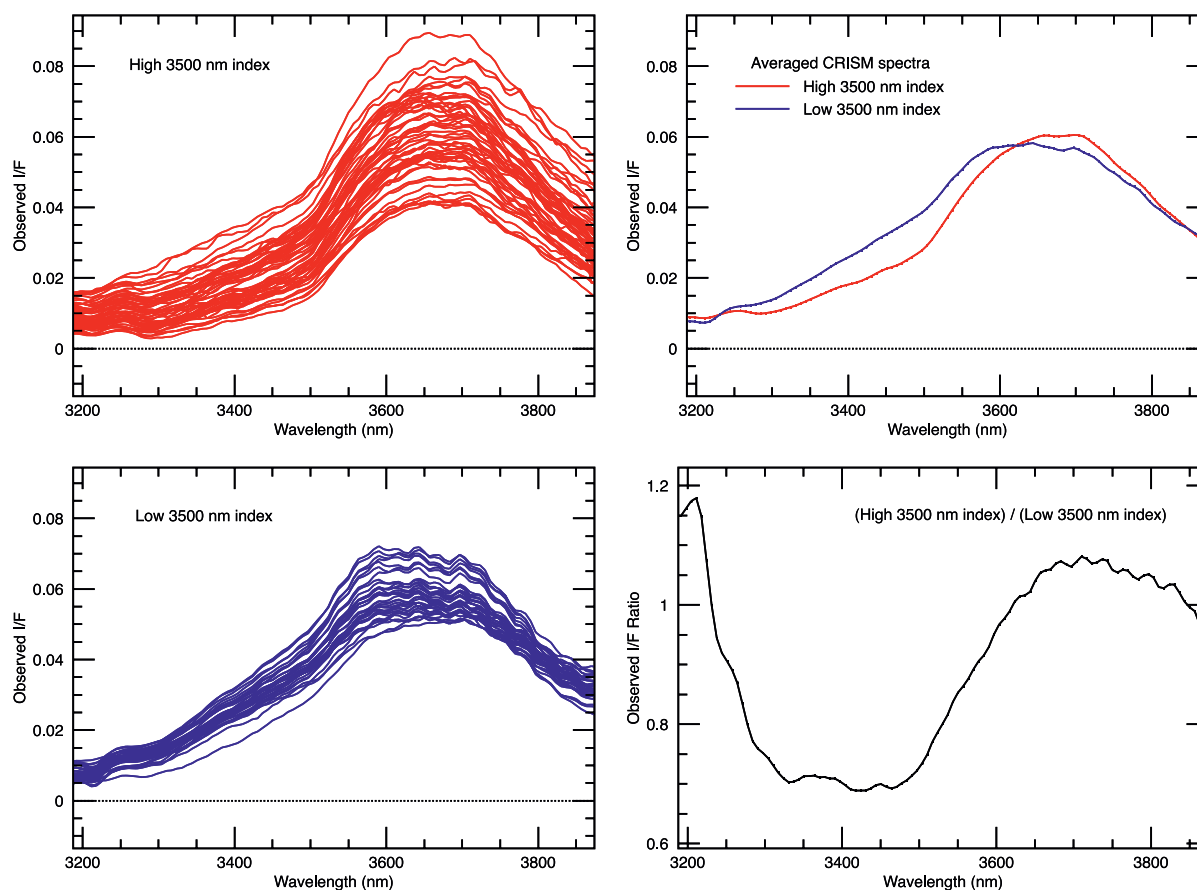


Figure 13. The results of the search for the spectral signature of H_2O_2 in Compact Reconnaissance Imaging Spectrometer for Mars (CRISM) spectra taken over H_2O surface ice. (Upper left) CRISM spectra containing relatively high values of 3,500 nm index (see text). (Lower left) CRISM spectra containing relatively low values of the 3,500 nm index. (Upper right) A comparison of the average spectra for all of the “high 3,500 nm index” and all of the “low 3,500 nm index” cases. (Lower right) The ratio between the “high 3,500 nm index” and “low 3,500 nm index” average spectra. This spectral dependence does not correspond to H_2O_2 . Instead, it is indicative of the presence of H_2O ice clouds.

future work. Obviously, also more searches should be undertaken, and complemented with searches for the H_2O_2 signature in UV spectra.

6. Potential Irreversible Heterogeneous Reactions on Mars

6.1. Introduction

In terrestrial atmospheric science, research into the role of particulate matter on chemistry has increased over the past few decades. Polar ozone loss was a main driver for this increase (Solomon, 1999), but the research and applications are now widely spread to many aspects of atmospheric chemistry (George et al., 2015; Kolb et al., 2010). IUPAC has published an exhaustive overview of heterogeneous processes relevant for terrestrial—tropospheric—conditions, that were investigated in laboratory experiments (Ammann et al., 2013; Crowley et al., 2010). IUPAC provides preferred parameterizations for each type of reaction after consideration of all related experimental conditions and results. This database is regularly updated following new research (<https://iupac.aeris-data.fr>). It complements the NASA-JPL database that focuses more on stratospheric and upper atmospheric conditions (Burkholder et al., 2019; <https://jpldataeval.jpl.nasa.gov>).

The Martian atmosphere is comparable to the terrestrial stratosphere for temperature, pressure and humidity, but in terms of dust content, it can be more similar to the terrestrial troposphere in dusty conditions. For example, Dickinson et al. (2011) compared in situ lidar observations of dust on Earth (desert conditions) and Mars and found comparable dust content. However, the role of mineral dust on atmospheric chemistry on Mars has not been investigated at large scale since the 1D model results of Anbar et al. (1993). Experimental knowledge about heterogeneous

Table 3

List of Heterogeneous, Irreversible Uptake, Reactions Recommended by International Union of Pure and Applied Chemistry (Taken From Crowley et al., 2010 or for Later Updates: <https://iupac.aeris-data.fr>) for Atmospheric Applications on Earth, and Considered in the Present Study for Mars

Molecule	Uptake coefficient (γ)	Temperature (K)	Concentration (laboratory)	Maximum concentration (Mars)	Latest evaluation
Reactions on mineral dust					
OH	0.2	280–320	10^{-7} – 10^{-4} mbar	10^{-10} mbar	June 2017
HO ₂	3×10^{-2}	280–320	10^{-9} – 10^{-7} mbar	10^{-8} mbar	June 2016
H ₂ O ₂	10^{-4}	268–320	10^{-6} – 10^{-3} mbar	10^{-6} mbar	June 2017
O ₃	$1,500 \times [\text{O}_3]^{-0.7}$	298	10^{10} – 10^{15} cm ⁻³	10^{11} cm ⁻³	June 2016
Reactions on water ice					
OH	0.03	205–230	10^{-6} mbar ^a	10^{-10} mbar	December 2007
HO ₂	[0.025] ^b	223	10^{-6} mbar ^a	10^{-8} mbar	February 2008
O(³ P)	$7 \times 10^{-6} + 2.6 \times 10^{-24} \times \exp(1,370/T) \times [\text{O}_2]$	110–150	$[\text{O}_2] < 10^{14}$ cm ⁻³	$[\text{O}] \sim 10^8$ cm ⁻³ $[\text{O}_2] < 10^{15}$ cm ⁻³	June 2014
O ₃	$< 10^{-8}$	220–260	10^8 – 10^{12} cm ⁻³	10^{11} cm ⁻³	December 2007

^aTaken from Abbatt (2003). ^bNot recommended by IUPAC.

processes on dust—as well as on ice—has massively increased over these past three decades, as the IUPAC reports testify. We use the IUPAC recommendations as a starting point to investigate heterogeneous processes on Mars, acknowledging that it is unknown to what degree the properties of Martian and terrestrial dust correspond.

6.2. Reactions Recommended by IUPAC

Of all heterogeneous reactions listed by IUPAC, we initially limit ourselves to reactions on solid surfaces (Crowley et al., 2010), and more specifically to mineral dust and water ice. While liquid substrates may exist on Mars (such as brines (e.g., Rivera-Valentin et al., 2020) and deliquescent perchlorate salts (e.g., Nikolakakos and Whiteway, 2015, 2018)), for now we consider their prevalence as too sparse to have any impact on global scale chemistry. We also only consider molecules known to be present on Mars and included in the GEM-Mars model (Daerden et al., 2019). For the moment, we are ignoring nitrogen compounds, which are expected to have a secondary role in controlling ozone abundances compared to the HO_x chemistry (Lefèvre and Krasnopolsky, 2017), as well as the recently discovered chlorine chemistry (Aoki et al., 2021; Korablev et al., 2021). Specifically, we are considering OH, HO₂, H₂O₂ and O₃ for reactions on mineral dust, and OH, HO₂, H₂O₂, O(³P) and O₃ for reactions on water ice.

We do not consider the uptake of H₂O on ice as this would interfere with our simple cloud scheme. The chosen list of uptake reactions considered here is shown in Table 2.

6.3. Uptake Reactions on Mineral Dust

Dust is ubiquitous on Mars and continuously present. It therefore has the potential to provide a stable and significant surface presence for heterogeneous reactions. On Earth, a wealth of heterogeneous reactions on many types of mineral dust and comparable particles (e.g., clays, sands, mineral oxide surfaces, quartz, soot) have been identified (Crowley et al., 2010, and references therein).

Most of the data on trace gas-dust interactions was collected at room temperature (Table 3), so there will be some uncertainty related to the use of the measured coefficients for Mars. Uptake to solid surfaces is generally favored at low temperatures as surface-accommodation into a potential well (i.e., the initial step in uptake) is favored by low collisional energy and by reduced rates of (physi-)desorption. Therefore, we expect that the uptake will increase with decreasing temperatures, and so that the reported uptake coefficients in Table 3 likely represent a lower limit.

The uptake coefficients for HO₂, H₂O₂, and O₃ interacting with mineral dust were measured using concentration ranges that have overlap with Mars concentrations as simulated in the GEM-Mars model. Only the uptake of OH was measured for concentrations far above the values simulated for Mars.

6.4. Uptake Reactions on Water Ice

Opposite to the uptake on dust, the experiments for uptake on ice were all done at temperatures that are within the range of temperatures found in the atmosphere of Mars (Table 3).

The reactions of OH and HO₂ were studied at partial pressures above 10⁻⁶ mbar (Abbatt, 2003; Cooper & Abbatt, 1996) which is orders of magnitude larger than the highest Martian concentrations (the impact will be discussed below). The uptake of O(³P) does not cite specific concentrations, but was measured as a function of the O₂ concentration, and this was within the range of O₂ concentrations simulated on Mars. The uptake of O₃ was measured for concentrations that also fall in the range of Martian O₃ concentrations. However, this reaction was reported by IUPAC as not very efficient, and only a (low) upper limit to the uptake coefficient is recommended.

Cooper and Abbatt (1996) measured the uptake of OH (at 205–230 K) and HO₂ (at 223 K) on water ice. The uptake coefficients (γ) were used in several studies for Mars (Lefèvre et al., 2008, 2021) with considerable success, as by reducing HO₂ this reaction allowed simulation of larger total ozone columns in specific seasons and latitude ranges, and resulted in a better agreement with observations. However this success was not universal, as the improvement was not confirmed in all cases (Clancy et al., 2016, 2017; Lefèvre et al., 2021), in spite of model improvements (Lefèvre et al., 2021). Nevertheless, the work of Lefèvre et al. (2008, 2021) was the first to strongly demonstrate the potential impact of heterogeneous processes on Mars.

IUPAC does not recommend the uptake coefficient of HO₂ on water ice ($\gamma = 0.025$) for terrestrial atmospheric studies, and this for several reasons. The experimental database for the uptake of HO₂ to ice surfaces is very weak. In the only experimental study (Cooper & Abbatt, 1996), HO₂ levels were employed (5×10^{10} molecules cm⁻³, or 10⁻⁶ mbar) that far exceed those found in the atmosphere. If, by analogy to OH uptake, the surface reaction is driven by accommodation of HO₂ followed by its self-reaction, the net uptake coefficient obtained ($\gamma_{\text{HO}_2(\text{ice})} = 0.025$) is likely to be unique to the conditions of their experiment. Note that the rate of the self-reaction of HO₂ on the surface varies quadratically in HO₂, so that a factor 10 lower concentration will reduce the rate of self-reaction by a factor 100 with a related reduction in $\gamma_{\text{HO}_2(\text{ice})}$. For conditions where gas-phase HO₂ levels are lower than those used experimentally, the uptake coefficient of Cooper and Abbatt (1996) should strictly be regarded as an upper limit.

We can also gain insight into the validity of the Cooper and Abbatt (1996) uptake coefficients by examining experimental data on the uptake of HO₂ to aqueous surfaces (Ammann et al., 2013). While the accommodation coefficient (α) for the uptake of HO₂ to liquid water is large, $\gamma_{\text{HO}_2(\text{aq})}$ depends on the concentration of HO₂ (and O₂⁻) and on dissolved transition metal ions (TMI). At low HO₂ and for [TMI] = 0, $\gamma_{\text{HO}_2(\text{aq})}$ can be as low as 0.003. This is a factor of ~10 lower than obtained by Cooper and Abbatt (1996) for uptake to ice. We can speculate that this large enhancement for $\gamma_{\text{HO}_2(\text{ice})}$ compared to $\gamma_{\text{HO}_2(\text{aq})}$ may result from the different temperatures involved. Assuming a Langmuir-Hinshelwood type reaction, an increase in $\gamma_{\text{HO}_2(\text{ice})}$ at low temperatures would be driven by an increase in the surface coverage of HO₂ if the self-reaction of molecular HO₂ is the dominant loss process. In this case, for a given HO₂ level in the gas-phase the rate of HO₂ + HO₂ collisions at the surface will increase as the surface coverage increases at low temperature. If, as in the gas-phase, the self-reaction of surface bound HO₂ has a negative temperature dependence, this may amplify the effect. On the other hand, if the reaction on ice is driven by dissociation of HO₂ to O₂⁻, the colder temperatures (which result in less HO₂-mobility in surface layers) may slow down (or stop) the ionization of HO₂ and thus the subsequent reactions.

On balance, the use of an uptake coefficient of 0.025 for $\gamma_{\text{HO}_2(\text{ice})}$ is likely to result in a significant overestimation of the loss rates of HO₂ to ice surfaces at temperatures close to 223 K (and above) if the prevalent gas-phase HO₂ concentrations are lower than the experimentally deployed values of $\sim 5 \times 10^{10}$ molecules cm⁻³.

Inspired by these considerations, the true uptake coefficient for HO₂ on ice may well be a factor 10 lower than the one presented in Cooper and Abbatt (1996). In the subsequent simulations, we will also include the HO₂ uptake with a reduced value of γ to check whether this reaction would still be important.

6.5. Simulating Individual Uptake Processes

In order to understand the impact of each of the uptake reactions in Table 3, we simulated each one of them individually in a simulation based on the HPS model version (Table 2). The surface area densities (SAD) for dust and ice in the model are presented in Text S1 and Figures S6 through S9 in Supporting Information S1. We show the

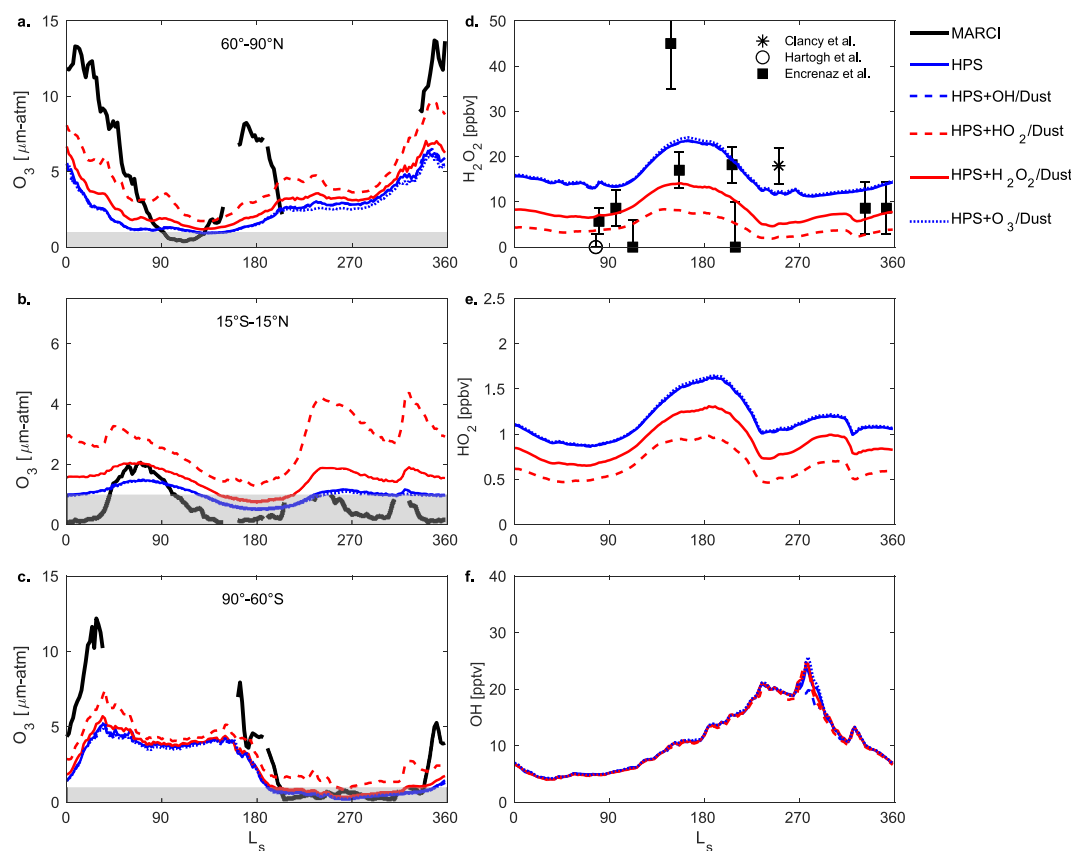


Figure 14. As Figure 6 but showing the simulations with heterogeneous processes on mineral dust for the species as indicated (see Table 2 for acronyms). All heterogeneous processes were added separately to the Hydrogen Peroxide Sublimation case in each simulation. All blue curves are overlapping.

results of these simulations for afternoon O_3 columns and daytime H_2O_2 and HO_x columns in Figure 14 for the reactions on mineral dust, and in Figure 15 for the reactions on water ice.

Only three processes have a visible impact: (a) the uptake of HO_2 on mineral dust (HPS + HO_2 /Dust), (b) the uptake of H_2O_2 on mineral dust (HPS + H_2O_2 /Dust), and (c) the uptake of HO_2 on ice following the Cooper and Abbatt (1996) coefficient (HPS + HO_2 /Ice). None of the remaining heterogeneous reactions have any impact on the global scale abundances of both species. We find that the uptake of OH on water ice (one of the two processes considered in the simulations applying the Cooper and Abbatt (1996) uptake coefficients) is not efficient in a standalone simulation.

For the uptake of HO_2 on mineral dust (HPS + HO_2 /Dust, red dashed line in Figure 14), we find that global dayside HO_2 abundances are reduced by 50%, resulting in a reduction of H_2O_2 of 75%. This brings the simulated H_2O_2 abundances below most of the available H_2O_2 detections, leaving it barely within the lower error bars of four detections, and within the upper limits of the non-detections. However, the higher detections in the middle of the year are underestimated. This then leads to a strong increase of the O_3 columns in the north, and a modest increase in the south. However, at the equator, the increase in ozone is too strong and brings it far above the observations.

For the uptake of H_2O_2 on mineral dust (HPS + H_2O_2 /Dust, red full line in Figure 14), we find that HO_2 is reduced by 25%, and H_2O_2 by 50%. However, this results only in a modest increase of the O_3 columns.

In sensitivity tests that keep track of the uptake of HO_2 and H_2O_2 by surface dust or airborne dust, or both, we found that airborne dust is the dominant substrate (see Figures S11 and S12 in Supporting Information S1). For the uptake of HO_2 on dust, uptake at the surface is negligible. For the uptake of H_2O_2 on dust, ~20% of the uptake occurs at the surface. On Earth, the surface was found to be a strong sink for H_2O_2 (e.g., Fischer et al., 2019 and references therein). Airborne dust is however much more abundant on Mars compared to the terrestrial locations considered in Fischer et al. (2019).

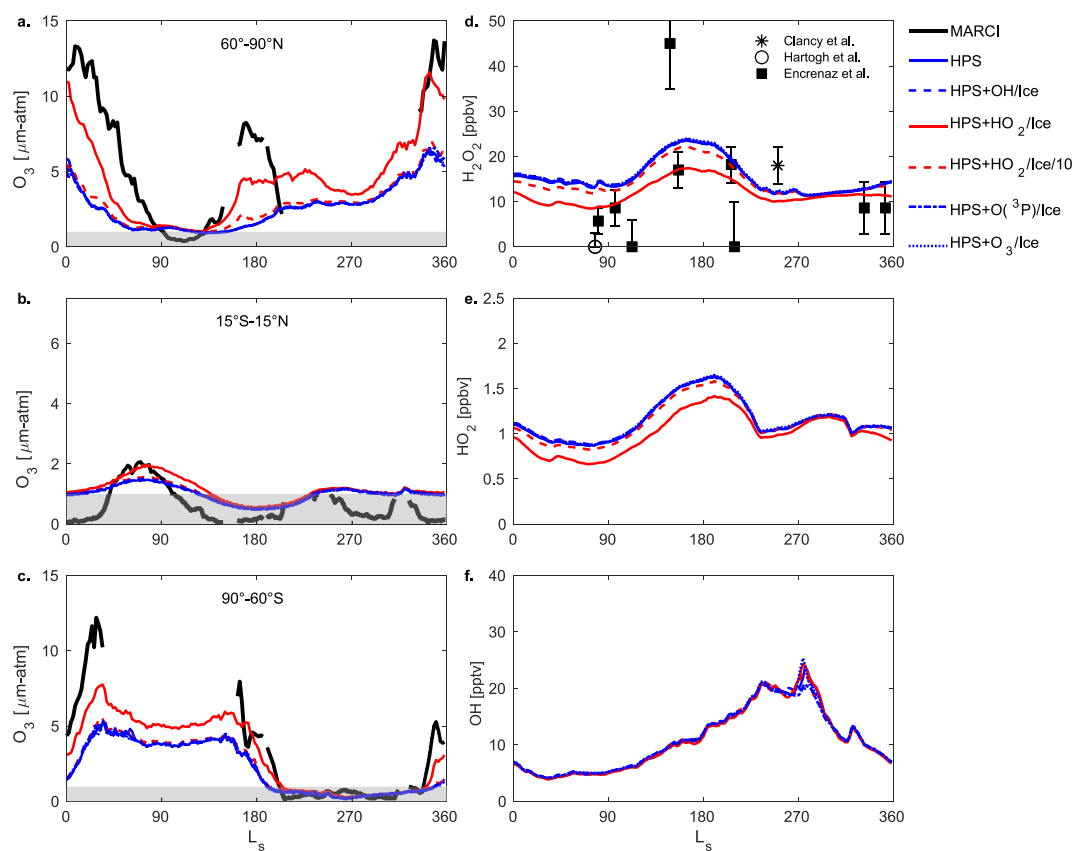


Figure 15. As Figure 6 but showing the simulations with heterogeneous processes on water ice for the species as indicated (see Table 2 for acronyms). All heterogeneous processes were added separately to the Hydrogen Peroxide Sublimation case in each simulation. All blue curves are overlapping.

For the HPS + HO₂/Ice case (Figure 15, red full line), global dayside HO₂ and H₂O₂ abundances are only slightly reduced, as the ice clouds form more locally compared to dust. However, O₃ columns are increased by amounts of up to 200% around the equinoxes in the north. At the equator and in the south, the O₃ increases are more modest. Comparable results were already found in previous work (Lefèvre et al., 2008, 2021).

We found that the effect of the uptake on CO₂ ice at the surface, using the same uptake coefficients as for water ice, was negligible (see Figure S13 in Supporting Information S1). In the present study, we did not consider uptake of HO₂ by CO₂ ice clouds.

This reaction applies the uptake coefficient for HO₂ on ice from Cooper and Abbatt (1996) and is not recommended by IUPAC (Section 6.4). When we scaled the uptake coefficient of HO₂ on ice down by a factor 10, we find that the impact of this reaction (Figure 15, red dashed line) is nearly negligible.

7. Impact of Water Ice Clouds on Photolysis Rates

An alternative or additional impact of water ice clouds on ozone abundances may relate to their ability to affect photolysis rates. Clouds act to attenuate the flux on material below the clouds but also to reflect sunlight, increasing the photolysis above the clouds. In terrestrial atmospheric models, such processes have been implemented with various levels of complexity (Flemming et al., 2015; Hall et al., 2018; Kim et al., 2015; Ryu et al., 2017). On Mars, Lindner (1988) considered this effect in a 1D model and found that it had only a limited impact.

Daerden et al. (2019) included the attenuation of sunlight by water ice clouds and its impact on photolysis rates below the clouds on Mars. This was implemented in the same way as attenuation by dust is treated, that is, by assuming spherical symmetry to calculate the optical paths (following the method of Brasseur & Solomon, 2005, Box 4.1). On Mars the dust distribution can be expected to usually be spherically symmetric. For attenuation

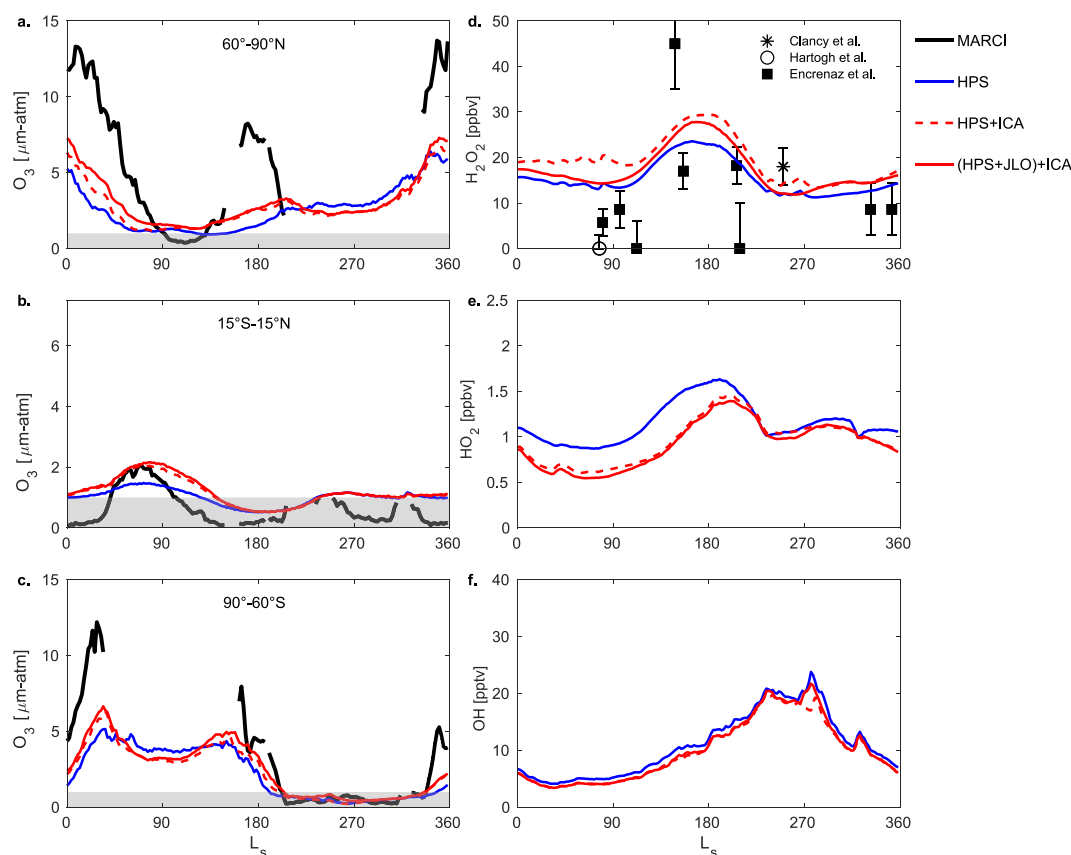


Figure 16. As Figure 6 but showing simulations with ice cloud attenuation applied to the Hydrogen Peroxide Sublimation (HPS) simulation (red dashed lines) and to the HPS simulation with photolytic loss of H_2O_2 in ice (red full lines).

by water ice clouds, it is more complicated as such an assumption would only be valid in case of meso- or large scale clouds, that is, it represents an extreme case of full regional cloud cover, as opposed to no clouds. However, applying the true 3D distribution of clouds to calculate the photolysis at every grid point would drive the computational cost to unrealistic values.

Figure 16 shows the results for the simulation with full ice cloud attenuation (ICA) (HPS + ICA) as compared to the simulation without no ICA (HPS). The HPS + ICA simulation produces more H_2O_2 and often also more O_3 than the HPS simulation, but less HO_2 . When also the photolytic loss of H_2O_2 in ice is included ((HPS + JLO) + ICA), O_3 abundances increase somewhat more.

8. Combination of the Proposed Processes and Reactions

Combining the various processes proposed in this paper may increase, or counteract, the impact of the individual processes. For example, combined uptake of HO_x and H_2O_2 on both dust and ice may remove more odd hydrogen from the atmosphere and lead to increased ozone abundances. Here, we present simulations that contain all of the heterogeneous reactions introduced in Sections 4 and 6, that is, irreversible uptake of HO_x , O_x , and H_2O_2 on mineral dust and water ice, and reversible BET-type adsorption of H_2O_2 on water ice. Then, these simulations are extended with the processes introduced in Sections 5 and 7, that is, photolytic destruction of H_2O_2 in ice, and attenuation of sunlight by water ice clouds.

Following the discussion in Section 6.4, we only consider the uptake of HO_2 on ice with an uptake coefficient reduced by a factor 10. Figure 17 shows the resulting simulations. The basic simulation (HPS + HET(HO_2 /Ice/10), blue dashed lines) strongly reduces the HO_2 and H_2O_2 abundances, with the latter being below most of the available H_2O_2 observations, and only in accordance with the non-detections. This results in a considerable increase of the global ozone abundances. In the polar regions, this leads to a better agreement with observations

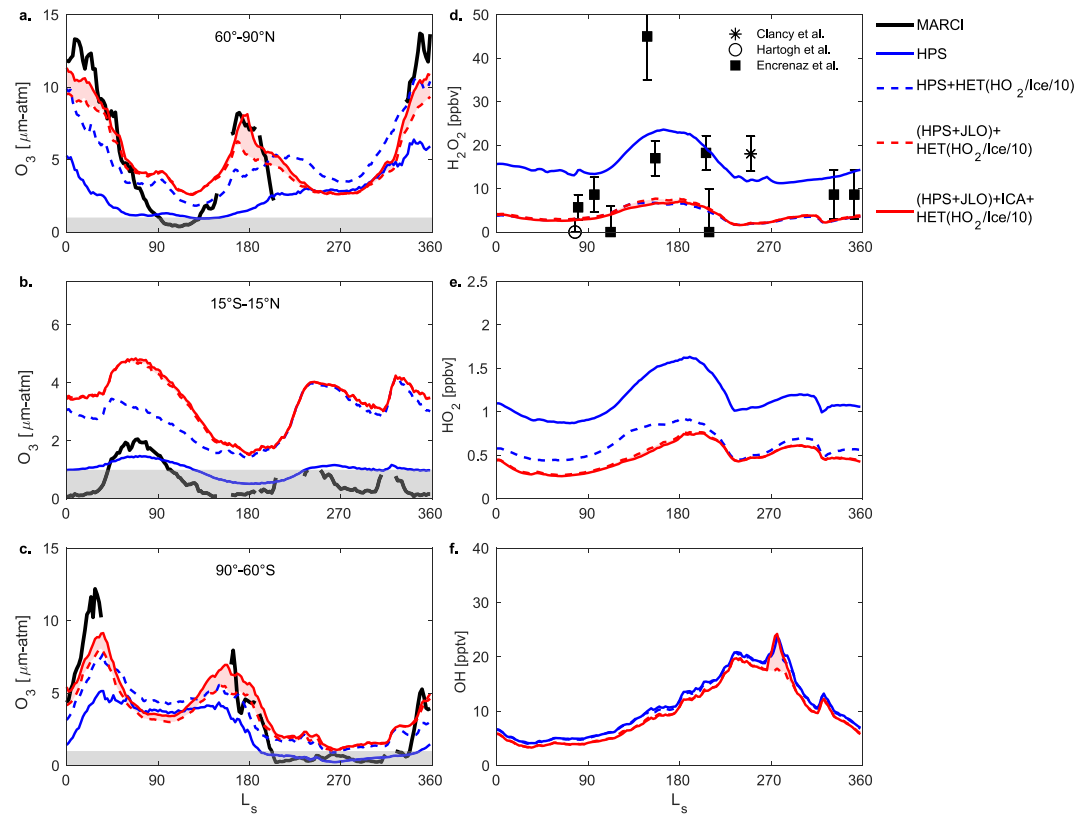


Figure 17. Set-up as Figure 6 but showing combinations of various processes introduced in this paper. The red shading indicates the range of impact that ice cloud attenuation could have, depending on the actual regional cloud cover.

around the equinoxes and during springtime. However, at the equator, and also in the north around summer solstice, the ozone abundances are too large compared to observations.

When photolytic loss of H_2O_2 in ice (both the condensed and adsorbed states) is included ((HPS + JLO) + HET($\text{HO}_2/\text{Ice}/10$), red dashed lines), HO_2 abundances are further reduced while H_2O_2 abundances stay the same. Ozone abundances are further increased in the polar regions around the equinoxes, and at the equator during the aphelion season. When also attenuation of sunlight by water ice clouds is included ((HPS + JLO) + ICA + HET($\text{HO}_2/\text{Ice}/10$), red full lines), there is no change in HO_x or H_2O_2 , but the peak ozone abundances in the polar regions are even more increased, and they approach the peak observations. However, at the equator, and also in the north around summer solstice, the ozone abundances remain too large compared to observations.

While these combined simulations can now almost reproduce the highest observed ozone columns, they severely overestimate the lowest ozone columns. There can be various causes for this overestimation:

- at the times and places of the overestimation of ozone by the model, the water vapor columns in the model are too low compared to observations (see Figure S3 in Supporting Information S1);
- the GEM-Mars model currently does not allow for supersaturation, which was found by Fedorova et al. (2020). This will make the model typically too dry in the middle and upper atmosphere (see Figure S5 in Supporting Information S1), and can contribute to excessive ozone in the equatorial region around aphelion, when the ozone column has important contributions from the middle atmosphere;
- the effect of cloud attenuation is likely too strong at the equator in the aphelion season, where clouds are likely less regionally extended compared to the polar hood clouds;
- the uptake of HO_2 on dust was found to have a large impact (see Section 6.3), possibly implying that the uptake coefficient measured on terrestrial dust may be too large for Mars.

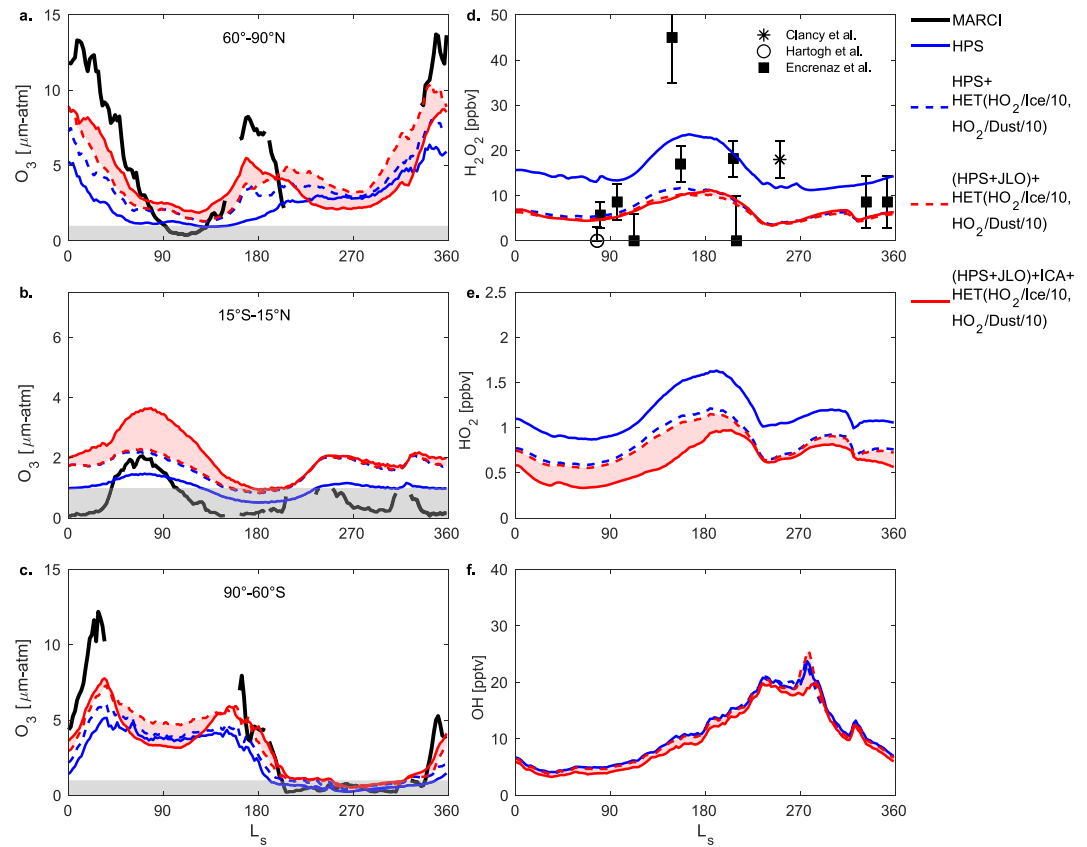


Figure 18. As Figure 17 but with reduced uptake of HO₂ on dust.

The first three problems require important model improvements related to water ice cloud formation and these are foreseen in the near future.

Here, we will show how the ozone simulations evolve when the uptake coefficient of HO₂ on dust is reduced. Figure 18 shows the simulations similar to those in Figure 17 but now also with uptake coefficient of HO₂ on dust reduced by a factor 10. Global scale HO₂ and H₂O₂ abundances increase, bringing the latter closer to the observations—but still too low—while ozone abundances uniformly decrease on the global scale. This improves again the comparison with the lowest observed columns, but leads to an underestimation of the peak ozone columns, which was the problem we started with. But, there is a clear improvement over the pure homogeneous case (HPS), without involving strong uptake of HO_x by water ice clouds.

A more complete comparison of the zonal mean local afternoon O₃ columns from the (HPS + JLO) + HET(HO₂/Ice/10, HO₂/Dust/10) simulation (denoted as FINAL) to MARCI observations, as well as to the HPS and HPR + C&A simulations, is shown in Figure 5.

9. Discussion and Recommendations for Future Work

9.1. Discussion

By combining the proposed processes (Figure 17), we were able to simulate peak O₃ abundances similar to those in the simulation that included strong uptake of HO₂ on ice (HPS + C&A, Figure 6), but without using a potentially too large uptake coefficient.

On the other hand, the simulated O₃ columns still remain below the highest observed columns at high latitudes, while they are also excessive at low- and midlatitudes, and around the north pole in summer. This could be improved by reducing the uptake of HO₂ on dust (Figure 18), but this implies that the highest O₃ columns decrease again.

The comparison to the sparse set of available H₂O₂ observations remains an important additional constraint for the simulated processes. But in the case of the best O₃ simulation, the simulated H₂O₂ columns remain low compared to most of the available observations.

Obviously, combining a wide range of heterogeneous reactions, does not lead to a simple solution for the Mars ozone deficit problem.

The remaining biases for the ozone columns are at least partially due to the imperfect simulation of the water vapor abundances in the current model version. This will require model improvements in ice cloud microphysics.

There may also be uncertainties in the simulated dust SAD. However, as dust is ubiquitous on Mars, it can be expected to form a stable background throughout the atmosphere, with well-constrained size distributions dominated by particles of ~1.5 μm radius (e.g., Clancy et al., 2003). The total dust columns in the model are constrained by the daily maps of Montabone et al. (2015) that are constructed from observations. Therefore, it would be hard to imagine an uncertainty in the SAD of an order of magnitude or more, as can be the case on Earth (e.g., Bauer et al., 2004).

It may also be possible that Martian dust has undergone considerable chemical aging (e.g., Gaston, 2020) during perhaps millions of years or more. By chemical aging, we mean the alteration of the dust particles' surface coating and its chemical characteristics by long-term exposure to irreversible uptake of reactive gases and UV radiation. This aging can have changed the chemical characteristics of Martian dust so much that it can have become much less reactive than terrestrial dust.

As a result, our work does not provide definitive answers to the Mars ozone deficit problem, and actually rises even more questions. But our approach allows us to point to the specific investigations required for further understanding. These investigations comprise new observations, new laboratory experiments, and advancements in numerical modeling. We discuss each of these topics in some more detail below.

9.2. Recommendations for Future Work

9.2.1. Need for More Observations of H₂O₂ and HO_x

To properly evaluate all the considered processes on Mars, determining the abundance of odd hydrogen (HO_x) species, which are considered to be the invisible drivers of the Martian atmospheric chemistry, is critically needed. These species (HO₂ and OH) have never been directly observed on Mars, as their abundances are predicted to be quite low, at respectively ppbv and pptv levels (Figure 6). The presence of OH was confirmed by detecting airglow from OH Meinel band emission (Clancy et al., 2013). An Earth-based search for HO₂ by Villanueva et al. (2013) was negative but with a high upper limit. The predicted HO₂ abundance is near the detection limit of instruments on the ExoMars Trace Gas Orbiter (TGO) mission: NOMAD (Robert et al., 2016; Vandaele et al., 2018, 2019) and ACS (Korablev et al., 2018, 2019). However, HO₂ has not been detected in the first 5 years of the TGO science mission.

H₂O₂ is a more abundant (~10 ppbv), relatively stable reservoir species of HO_x, that is observable in the IR (~8 μm) and sub-millimeter spectral ranges. Between 1988 and 2018, 12 detection efforts were reported in the literature (11 Earth-based, Clancy et al., 2004; Encrenaz et al., 2019; Krasnopolsky et al., 1997, and 1 space-based, Hartogh et al., 2010), which included 4 non-detections. The non-detection in 1988 (Krasnopolsky et al., 1997) with an upper limit of 30 ppbv, occurred in the same season ($L_s \sim 200^\circ$ – 250°) as the consistent, positive detections by Clancy et al. (2004) and Encrenaz et al. (2019) of ~15–20 ppbv. Of the 8 detections, 6 were considerably (factor of 2) revised in 2019 (Encrenaz et al., 2019). Of the two remaining, unrevised, detections, one is much larger than any other reported detection (45 ± 10 ppbv at $L_s = 148^\circ$, Encrenaz et al., 2019). Two of the revised values (17 ± 4 ppbv at $L_s = 156^\circ$, and 18.2 ± 4 ppbv at $L_s = 206^\circ$) are very close in terms of L_s to other observations with very different values. This is unexpected, as the Martian atmosphere and its chemical composition are known to be highly annually repeating (outside of global dust storm events), for example, Clancy et al. (2016), Smith et al. (2018).

In comparison to other trace gases on Mars, such as H₂O, CO, O₂, O₃, and even HCl (which is less abundant than H₂O₂, Aoki et al., 2021; Korablev et al., 2021), the observational record for H₂O₂ is extremely limited and inconclusive in terms of seasonal trends and spatial distribution. As a consequence, the currently available H₂O₂

data set does not allow to draw any firm conclusions on the processes discussed in this paper. More, and more accurate, observations of H_2O_2 are urgently needed to advance our understanding of Mars' atmospheric chemistry. One of the purposes of the present paper is to bring this problem to the attention of the Martian and planetary community, in particular the observational community and space mission proposal and planning teams.

No previous or planned space mission to Mars was or is able to detect H_2O_2 . This is partially due to the cancellation or non-selection of proposed sub-millimeter sounders on Mars missions (e.g., Zurek et al., 2011), while IR sounders either did not target the wavelength domains relevant for H_2O_2 , or did not have sufficient spectral resolution. One exception was the TIRVIM sounder on ACS on TGO (Korablev et al., 2018), but TIRVIM was taken out of service within the first MY of the mission (e.g., Fan et al., 2022), and no H_2O_2 detection was reported.

Given the lack of inclusion of H_2O_2 sensitive instruments on planned space missions, the community may have to rely on ground-based measurements to address a critical problem in Mars atmospheric chemistry. The Atacama Large Millimeter Array (ALMA) facility provides a unique platform with unsurpassed accuracy, and even with unsurpassed spatial (horizontal and vertical) resolution to observe H_2O_2 in the sub-millimeter range. Parks et al. (2021) discussed the potential for horizontal mapping of the Martian atmosphere using ALMA. But ALMA's high spatial resolution will also enable spatially resolved observations of the limb of the Martian disk. In such a limb viewing mode, the sampled atmospheric mass is more than an order of magnitude larger than in nadir viewing mode, while the background is deep space, and so this does not suffer from complications related to the surface emissivity and thermal contrasts that the nadir viewing mode encounters. Thus, we strongly encourage observational teams to submit proposals to detect H_2O_2 with ALMA in limb viewing mode.

Apart from having more accurate detections of H_2O_2 , it is also important to fill the gaps in the observational record throughout the Martian year (Figure 6), in order to get a better knowledge about the actual seasonal cycle, and if possible, to contribute to evaluating and perhaps discerning the different processes considered in this paper.

In addition, we tentatively started a search for H_2O_2 deposits in surface ices on Mars, inspired by similar work done for the Jovian moons Europa (Carlson et al., 1999; Hand and Brown, 2013) and Ganymede (Trumbo et al., 2023). In this first effort, using CRISM spectra, we did not find the signature of H_2O_2 , which could be consistent with the photolytic loss of H_2O_2 in ices proposed in our paper (inspired by Loeffler et al., 2013). However, simulated spectra are needed to quantify this result, and should be calculated. We also recommend future searches for H_2O_2 in Mars surface ices, including with UV spectrometers.

9.2.2. Need for More Laboratory Experiments

For our study, we rely on the laboratory data taken under terrestrial atmospheric conditions, which only in some cases overlapped with Mars atmospheric conditions (Table 3). Currently, the most crucial value relevant to Mars is the uptake coefficient of HO_2 on water ice ($\gamma = 0.025$), as this is the single reaction that can largely explain ozone abundances on Mars. However, as noted earlier, the accuracy of this value is questionable and needs to be repeated for atmospheric conditions. If its true value is much smaller, as is likely, its impact is almost negligible.

The most efficient reactions found in our simulations are the uptake of HO_2 and H_2O_2 by mineral dust, where we assumed the recommended uptake coefficients for the terrestrial atmosphere of respectively $\gamma = 0.03$ and $\gamma = 0.0001$. These uptake coefficients were obtained at temperatures close to 300 K, and would represent a lower limit for the same dust at Martian temperatures. However, their impact on the simulated global abundances of H_2O_2 and O_3 is too large, at least for the uptake of HO_2 . This may relate to chemical aging of Martian dust, which may have made Martian dust less reactive compared to terrestrial dust. The increasing potential to investigate real Martian dust in-situ by lander missions (e.g., Berger et al., 2016) or from sample returns, will allow future studies on the composition of Martian dust as well as its reactive properties. Also laboratory experiments on Earth mimicking the Martian environment, as well as theoretical quantum-mechanical calculations and simulations, could provide insights on the process of chemical aging of dust under Martian circumstances.

While we did not find that the adsorption of H_2O_2 on water ice had an impact on resulting ozone abundances, even using a BET isotherm, the exact isotherm for the adsorption at low temperatures and pressures remains unknown. Considering that the theoretical work of Picaud and Jedlovszky (2014) indicates that the adsorption may depend strongly on the type of adsorption that occurs, this should be investigated in future laboratory experiments.

Also of importance is a better understanding of the low temperature behavior of H_2O_2 , its saturation vapor pressure over its solid, its solid state, and how it interacts with water (vapor and ice) at low temperatures and pressures.

Work done for ices on the Jovian moons (Loeffler and Baragiola, 2005, 2011) has been helpful in this respect, and should be extended to Martian conditions.

Finally, CO₂ ice is a highly abundant substrate in the seasonal polar caps on Mars, but also in polar precipitation (Kuroda et al., 2013), so also heterogeneous reactions on CO₂ ice should be investigated in laboratory experiments.

9.2.3. Need for More Model Refinements

In this study, we have found that two processes have an important impact on the chemistry simulations: (a) the impact of water ice clouds on photolysis rates—this was only applied before in Lindner (1988) in a 1D model, and in Daerden et al. (2019), Daerden, Neary, Wolff, et al. (2022) in a 3D model—and (b) the photolytic loss of H₂O₂ in its solid and adsorbed states.

For the impact of water ice clouds, we implemented the attenuation below the clouds assuming full spherical symmetry of the overhead clouds. This may be valid in some regimes (e.g., large-scale clouds within the polar hood), but will not be accurate in the case of less dense cloud coverage (e.g., in the ACB, and at the edges of the polar hoods). Low computational cost parameterizations to refine this implementation should be developed. For instance, a cloud cover index could modulate the attenuation effect. In addition, reflectance above the clouds should be considered.

Using the photolysis rate coefficients calculated for the gas-phase model, and applying it as a loss rate to the mixing ratio tracer of the condensed and adsorbed states, we implemented photolytic loss of H₂O₂ in its solid and adsorbed states. However, we did not include specific information about the particles or substrates (shape, composition, mixtures, vertical distribution in the surface ice), which could be refined in future work. Also subsequent reactions of the photolysis products (OH radicals) in the ice should be considered.

Given the importance of particulate matter for heterogeneous processes, the current implementation of dust and water ice clouds in the GEM-Mars model is very simplistic compared to other models (e.g., Haberle et al., 2019; Navarro et al., 2014). Currently, we are developing a full microphysical model in the GCM based on the work of Daerden et al. (2010), which will allow for a more refined (highly size-resolved) representation of dust and ice particles that act as substrates, enabling us to assess its impact on the heterogeneous processes.

It will also allow to improve the calculated seasonal, column-integrated and vertical water vapor, dust and ice distributions, which are very important constraints for the simulated minor species and the heterogeneous processes. In particular, an important question is how the model-data biases for ozone will improve if the model will be better capable of reproducing the observed water vapor distributions (Figure S3 in Supporting Information S1). In addition, the impact of these improvements on the vertical distributions can be investigated by coincident profile measurements of dust, water ice, H₂O and O₃ by the NOMAD instrument suite on the ExoMars TGO (Aoki et al., 2019, 2022; Daerden, Neary, Wolff, et al., 2022; Khayat et al., 2021; Patel et al., 2021; Piccialli et al., 2023).

Finally, microphysical modeling approaches for H₂O₂-H₂O mixtures should be explored, as currently the behavior of H₂O₂ in its solid state and in mixtures with water ice is not fully understood.

10. Summary

We have illustrated some of the complexity in Mars atmospheric chemistry, including gas-particle (dust and ice) interactions. Some of these interactions are direct (uptake, adsorption), while others are more complex and deal with interaction of particles with sunlight.

H₂O₂ is peculiar as it is a reservoir species of HO_x but is also the only species on Mars that deposits under conditions similar to water vapor. This requires a careful approach for its implementation in modeling, and we presented the first such approach in this paper. We have argued and partly illustrated that the interaction with water (vapor, ice) at low temperature may be complicated (adsorption, deposition/sublimation, hydrate formation), and may have an important impact on HO_x and O₃ chemistry.

We also tried to export knowledge about heterogeneous processes on Earth to Mars. For water ice, the substrates should be similar, but for mineral dust, this may not be the case, suggesting more work needs to be done to know the limits of using terrestrial mineral dust results for Mars.

We summarize the main messages from our work below:

1. The uptake coefficient of HO₂ on water ice (Cooper & Abbatt, 1996), that was crucial to improve ozone simulations in models, may be too large.
2. For all of the other heterogeneous reactions considered, we find that the uptake of HO₂ and H₂O₂ on dust may be very efficient. For HO₂, the simulated uptake seems too strong, which may indicate that Mars dust has undergone significant chemical aging over time.
3. Previous models implemented removal of H₂O₂ after it saturates but without a clear physical process. Here, we propose that solid phase H₂O₂ can be efficiently destroyed by photolysis. Photolysis also removes H₂O₂ from polar ices, including the permanent cap, and even during polar winters, as we demonstrated that the main source of polar H₂O₂ deposits is precipitation from atmospheric particles that were at some point exposed to sunlight.
4. Using spectra taken by CRISM, we found the absence of H₂O₂ in Martian surface ices, however we could not yet define detection limits.
5. We showed that attenuation of sunlight by water ice clouds has an important impact on photolysis rates and the resulting gas abundances.
6. We showed that combining the considered processes can increase ozone abundances without relying on strong uptake of HO₂ on ice. In these simulations, ozone is still too low at high latitudes compared to data, and too high at low latitudes.
7. We found that no proposed model simulation could uniquely reproduce all of the observations of H₂O₂ on Mars. However, more observations are needed to better understand which of these observations are representative of overall trends.

Finally, together with other insights gathered in this work, we are able to provide the following recommendations for future work and research that will help to unravel further the puzzle of Martian chemistry:

1. More observations of H₂O₂ are needed, including using the unique capabilities of the ALMA observatory. Observations should cover more Martian seasons and fill gaps in the current data set. Observations should continue to search for H₂O₂ in Mars polar ices. Future space missions should include the capability to detect H₂O₂ and HO₂.
2. More laboratory experiments are needed to better understand the low temperature behavior of H₂O₂ and its interaction with H₂O, and to better quantify heterogeneous reactions (uptake and adsorption of trace gases) under Martian conditions and for concentrations relevant for the Martian atmosphere, including on real, or realistic surrogates for, Martian dust samples, and on low temperature ices, including on CO₂ ice. Chemical aging of dust under Martian conditions should also be explored.
3. More refined parameterizations in models are needed to calculate the impact of water ice clouds on photolysis rates, and to calculate the photolytic loss of H₂O₂ in its solid and adsorbed states. More in general, improvements in the simulated distributions of water vapor and ice clouds are required to further improve the ozone simulations.

Data Availability Statement

The MARCI ozone data set presented in this work, as well as the results from the GCM simulations and the experimental results of Pouvesle et al. (2010), are available in this in-text data citation reference: Daerden et al. (2023). The CRISM data used in this paper are available on the Planetary Data System (PDS) Geosciences Node (Murchie, 2006).

The GEM-Mars General Circulation Model is based on the Global Environmental Multiscale model (GEM) 4.2.0 version of the community weather forecasting model for Earth, which is one of the more recent versions available to the community, under the GNU Lesser General Public Licence v2.1. The adaptation for Mars is developed and maintained at the Royal Belgian Institute for Space Aeronomy. Public information on the GEM-Mars model is being developed on <https://gem-mars.aeronomie.be/>.

This work was made possible thanks to the reconstructed gridded maps of column dust optical depth from Mars Climate Sounder observations provided by L. Montabone (Montabone et al., 2015, 2019). The dust maps were prepared using MCS v5.3 provided by A. Kleinböhl and D. Kass. Dust climatologies can be found at the following link: http://www-mars.lmd.jussieu.fr/mars/dust_climatology/.

Acknowledgments

The authors thank Franck Lefèvre and Vladimir Krasnopolsky for their constructive comments on the paper. This work acknowledges funding by the Belgian Science Policy Office (BELSPO), with the financial and contractual coordination by the ESA Prodex Office (PEA 4000103401, 4000121493). This work has received support from the European Union's Horizon 2020 research and innovation programme (grant agreement no. 101004052, RoadMap project).

References

Abbatt, J. P. D. (2003). Interactions of atmospheric trace gases with ice surfaces: Adsorption and reaction. *Chemistry Review*, *103*(12), 4783–4800. <https://doi.org/10.1021/cr0206418>

Ammann, M., Cox, R. A., Crowley, J. N., Jenkin, M. E., Mellouki, A., Rossi, M. J., et al. (2013). Evaluated kinetic and photochemical data for atmospheric chemistry: Volume VI—Heterogeneous reactions with liquid substrates. *Atmospheric Chemistry and Physics*, *13*(16), 8045–8228. <https://doi.org/10.5194/acp-13-8045-2013>

Anbar, A. D., Leu, M. T., Nair, H. A., & Yung, Y. L. (1993). Adsorption of HO_x on aerosol surfaces: Implications for the atmosphere of Mars. *Journal of Geophysical Research*, *98*(E6), 10933–10940. <https://doi.org/10.1029/93je00132>

Aoki, S., Daerden, F., Viscardi, S., Thomas, I. R., Erwin, J. T., Robert, S., et al. (2021). Annual appearance of hydrogen chloride on Mars and a striking similarity with the water vapor vertical distribution observed by TGO/NOMAD. *Geophysical Research Letters*, *48*(11), e2021GL092506. <https://doi.org/10.1029/2021GL092506>

Aoki, S., Vandaele, A. C., Daerden, F., Villanueva, G. L., Liuzzi, G., Clancy, R. T., et al. (2022). Global vertical distribution of water vapor on Mars: Results from 3.5 years of ExoMars-TGO/NOMAD science operations. *Journal of Geophysical Research: Planets*, *127*(9), e2022JE007231. <https://doi.org/10.1029/2022JE007231>

Aoki, S., Vandaele, A. C., Daerden, F., Villanueva, G. L., Liuzzi, G., Thomas, I. R., et al. (2019). Water vapor vertical profiles on Mars in dust storms observed by TGO/NOMAD. *Journal of Geophysical Research: Planets*, *124*(12), 3482–3497. <https://doi.org/10.1029/2019JE006109>

Atreya, S. K., & Gu, Z. G. (1994). Stability of the Martian atmosphere: Is heterogeneous catalysis essential? *Journal of Geophysical Research*, *99*(E6), 13133–13145. <https://doi.org/10.1029/94je01085>

Bauer, S. E., Balkanski, Y., Schulz, M., Hauglustaine, D. A., & Dentener, F. (2004). Global modeling of heterogeneous chemistry on mineral aerosol surfaces: Influence on tropospheric ozone chemistry and comparison to observations. *Journal of Geophysical Research*, *109*(D2), D02304. <https://doi.org/10.1029/2003JD003868>

Berger, J. A., Schmidt, M. E., Gellert, R., Campbell, J. L., King, P. L., Flemming, R. L., et al. (2016). A global Mars dust composition refined by the alpha-particle X-ray spectrometer in Gale crater. *Geophysical Research Letters*, *43*(1), 67–75. <https://doi.org/10.1002/2015GL066675>

Brasseur, G., & Solomon, S. (2005). *Aeronomy of the middle atmosphere*. Springer Verlag.

Brown, M. A. J., Patel, M. R., Lewis, S. R., Holmes, J. A., Sellers, G. J., Streeter, P. M., et al. (2022). Impacts of heterogeneous chemistry on vertical profiles of Martian ozone. *Journal of Geophysical Research: Planets*, *127*(11), e2022JE007346. <https://doi.org/10.1029/2022JE007346>

Brunauer, S., Deming, L. S., Deming, W. E., & Teller, E. (1940). On a theory of the van der Waals adsorption of gases. *Journal of the American Chemical Society*, *62*(7), 1723–1732. <https://doi.org/10.1021/ja01864a025>

Brunauer, S., Emmett, P. H., & Teller, E. (1938). Adsorption of gases in multimolecular layers. *Journal of the American Chemical Society*, *60*(2), 309–319. <https://doi.org/10.1021/ja01269a023>

Burkholder, J. B., Sander, S. P., Abbatt, J., Barker, J. R., Cappa, C., Crouse, J. D., et al. (2019). Chemical kinetics and photochemical data for use in atmospheric studies, evaluation no. 19, JPL Publication 19-5, Jet Propulsion Laboratory, Pasadena. Retrieved from <http://jpldataeval.jpl.nasa.gov>

Carlson, R. W., Anderson, M. S., Johnson, R. E., Smythe, W. D., Hendrix, A. R., Barth, C. A., et al. (1999). Hydrogen peroxide on the surface of Europa. *Science*, *283*(5410), 2062–2064. <https://doi.org/10.1126/science.283.5410.2062>

Clancy, R. T., & Nair, H. (1996). Annual (perihelion–aphelion) cycles in the photochemical behavior of the global Mars atmosphere. *Journal of Geophysical Research*, *101*(E5), 12785–12790. <https://doi.org/10.1029/96je00836>

Clancy, R. T., Sandor, B. J., García-Muñoz, A., Lefèvre, F., Smith, M. D., Wolff, M. J., et al. (2013). First detection of Mars atmospheric hydroxyl: CRISM near-IR measurement versus LMD GCM simulation of OH Meinel band emission in the Mars polar winter atmosphere. *Icarus*, *226*(1), 272–281. <https://doi.org/10.1016/j.icarus.2013.05.035>

Clancy, R. T., Sandor, B. J., & Moriarty-Schieven, G. H. (2004). A measurement of the 362 GHz absorption line of Mars atmospheric H₂O₂. *Icarus*, *168*(1), 116–121. <https://doi.org/10.1016/j.icarus.2003.12.003>

Clancy, R. T., Smith, M. D., Lefèvre, F., McConnochie, T. H., Sandor, B. J., Wolff, M. J., et al. (2017). Vertical profiles of Mars 1.27 μm O₂ dayglow from MRO CRISM limb spectra: Seasonal/global behaviors, comparisons to LMDGCM simulations, and a global definition for Mars water vapor profiles. *Icarus*, *293*, 132–156. <https://doi.org/10.1016/j.icarus.2017.04.011>

Clancy, R. T., Wolff, M. J., & Christensen, P. R. (2003). Mars aerosol studies with the MGS TES emission phase function observations: Optical depths, particle sizes, and ice cloud types versus latitude and solar longitude. *Journal of Geophysical Research*, *108*(E9), 5098. <https://doi.org/10.1029/2003JE002058>

Clancy, R. T., Wolff, M. J., Lefèvre, F., Cantor, B. A., Malin, M. C., & Smith, M. D. (2016). Daily global mapping of Mars ozone column abundances with MARCI UV band imaging. *Icarus*, *266*, 112–133. <https://doi.org/10.1016/j.icarus.2015.11.016>

Clegg, S. M., & Abbatt, J. P. D. (2001). Uptake of gas-phase SO₂ and H₂O₂ by ice surfaces: Dependence on partial pressure, temperature, and surface acidity. *Journal of Physical Chemistry A*, *105*(27), 6630–6636. <https://doi.org/10.1021/jp010062r>

Cooper, P. L., & Abbatt, J. P. D. (1996). Heterogeneous interactions of OH and HO₂ radicals with surfaces characteristic of atmospheric particulate matter. *Journal of Physical Chemistry*, *100*(6), 2249–2254. <https://doi.org/10.1021/jp952142z>

Crowley, J. N., Ammann, M., Cox, R. A., Hynes, M. E., Jenkin, A., Mellouki, A., et al. (2010). Evaluated kinetic and photochemical data for atmospheric chemistry: Volume V – Heterogeneous reactions on solid substrates. *Atmospheric Chemistry and Physics*, *10*(18), 9059–9223. <https://doi.org/10.5194/acp-10-9059-2010>

Daerden, F., Crowley, J. N., & Wolff, M. J. (2023). Datasets and GEM-Mars simulations of ozone and H₂O₂ on Mars, for Daerden et al., 2023 [Dataset]. Royal Belgian Institute for Space Aeronomy (BIRA-IASB). <https://doi.org/10.18758/71021085>

Daerden, F., Neary, L., Villanueva, G., Liuzzi, G., Aoki, S., Clancy, R. T., et al. (2022). Explaining NOMAD/D/H observations by cloud-induced fractionation of water vapor on Mars. *Journal of Geophysical Research: Planets*, *127*(2), e2021JE007079. <https://doi.org/10.1029/2021JE007079>

Daerden, F., Neary, L., Viscardi, S., García Muñoz, A., Clancy, R. T., Smith, M. D., et al. (2019). Mars atmospheric chemistry simulations with the GEM-Mars general circulation model. *Icarus*, *326*, 197–224. <https://doi.org/10.1016/j.icarus.2019.02.030>

Daerden, F., Neary, L., Wolff, M. J., Clancy, R. T., Lefèvre, F., Whiteway, J. A., et al. (2022). Planet-wide ozone destruction in the middle atmosphere on Mars during global dust storm. *Geophysical Research Letters*, *49*(11), e2022GL098821. <https://doi.org/10.1029/2022GL098821>

Daerden, F., Whiteway, J. A., Davy, R., Verhoeven, C., Komguem, L., Dickinson, C., et al. (2010). Simulating observed boundary layer clouds on Mars. *Geophysical Research Letters*, *37*(4), L04203. <https://doi.org/10.1029/2009GL041523>

Dickinson, C., Komguem, L., Whiteway, J. A., Illnicki, M., Popovici, V., Junkermann, W., et al. (2011). Lidar atmospheric measurements on Mars and Earth. *Planetary and Space Science*, *59*(10), 942–951. <https://doi.org/10.1016/j.pss.2010.03.004>

Encrenaz, T., Bézard, B., Greathouse, T. K., Richter, M. J., Lacy, J. H., Atreya, S. K., et al. (2004). Hydrogen peroxide on Mars: Evidence for spatial and temporal variations. *Icarus*, *170*(2), 424–429. <https://doi.org/10.1016/j.icarus.2004.05.008>

- Encrenaz, T., Greathouse, T. K., Aoki, S., Daerden, F., Giuranna, M., Forget, F., et al. (2019). Ground-based infrared mapping of H₂O₂ on Mars near opposition. *Astronomy & Astrophysics*, 627, A60. <https://doi.org/10.1051/0004-6361/201935300>
- Encrenaz, T., Greathouse, T. K., Lefèvre, F., & Atreya, S. K. (2012). Hydrogen peroxide on Mars: Observations, interpretation and future plans. *Planetary and Space Science*, 68(1), 3–17. <https://doi.org/10.1016/j.pss.2011.03.019>
- Encrenaz, T., Greathouse, T. K., Lefèvre, F., Montmessin, F., Forget, F., Fouchet, T., et al. (2015). Seasonal variations of hydrogen peroxide and water vapor on Mars: Further indications of heterogeneous chemistry. *Astronomy & Astrophysics*, 578, A127. <https://doi.org/10.1051/0004-6361/201425448>
- Fan, S., Guerlet, S., Forget, F., Bierjon, A., Millour, E., Ignatiev, N., et al. (2022). Thermal tides in the Martian atmosphere near northern summer solstice observed by ACS/TIRVIM onboard TGO. *Geophysical Research Letters*, 49(7), e2021GL097130. <https://doi.org/10.1029/2021GL097130>
- Fedorova, A. A., Montmessin, F., Korablev, O., Luginin, M., Trokhimovskiy, A., Belyaev, D. A., et al. (2020). Stormy water on Mars: The distribution and saturation of atmospheric water during the dusty season. *Science*, 367(6475), 297–300. <https://doi.org/10.1126/science.aay9522>
- Fischer, H., Axinte, R., Bozem, H., Crowley, J. N., Ernest, C., Gilge, S., et al. (2019). Diurnal variability, photochemical production and loss processes of hydrogen peroxide in the boundary layer over Europe. *Atmospheric Chemistry and Physics*, 19(18), 11953–11968. <https://doi.org/10.5194/acp-19-11953-2019>
- Flemming, J., Huijnen, V., Arteta, J., Bechtold, P., Beljaars, A., Blechschmidt, A.-M., et al. (2015). Tropospheric chemistry in the integrated forecasting system of ECMWF. *Geoscientific Model Development*, 8(4), 975–1003. <https://doi.org/10.5194/gmd-8-975-2015>
- Foley, W. T., & Giguere, P. A. (1951a). Hydrogen peroxide and its analogues, II. Phase equilibrium in the system hydrogen peroxide-water. *Canadian Journal of Chemistry*, 29(2), 123–131. <https://doi.org/10.1139/v51-016>
- Foley, W. T., & Giguere, P. A. (1951b). Hydrogen peroxide and its analogues, IV. Some thermal properties of hydrogen peroxide. *Canadian Journal of Chemistry*, 29(10), 895–903. <https://doi.org/10.1139/v51-104>
- Gaston, C. J. (2020). Re-Examining dust chemical aging and its impacts on Earth's climate. *Accounts of Chemical Research*, 53(5), 1005–1013. <https://doi.org/10.1021/acs.accounts.0c00102>
- George, C., Ammann, M., D'Anna, B., Donaldson, D. J., & Nizkorodov, S. A. (2015). Heterogeneous photochemistry in the atmosphere. *Chemistry Review*, 115(10), 4218–4258. <https://doi.org/10.1021/cr500648z>
- Giguère, P. A. (1975). *Peroxyde d'hydrogène et polyoxydes d'hydrogène*. Elsevier Masson.
- Giguère, P. A., Liu, I. D., Dugdale, J. S., & Morrison, J. A. (1954). Hydrogen peroxide: The low temperature heat capacity of the solid and the third law entropy. *Canadian Journal of Chemistry*, 32(2), 117–128. <https://doi.org/10.1139/v54-019>
- Haberle, R. M., Kahre, M. A., Hollingsworth, J. L., Montmessin, F., Wilson, R. J., Urata, R. A., et al. (2019). Documentation of the NASA/Ames legacy Mars global climate model: Simulations of the present seasonal water cycle. *Icarus*, 333, 130–164. <https://doi.org/10.1016/j.icarus.2019.03.026>
- Hall, S. R., Ullmann, K., Prather, M. J., Flynn, C. M., Murray, L. T., Fiore, A. M., et al. (2018). Cloud impacts on photochemistry: Building a climatology of photolysis rates from the atmospheric tomography mission. *Atmospheric Chemistry and Physics*, 18(22), 16809–16828. <https://doi.org/10.5194/acp-18-16809-2018>
- Hand, K. P., & Brown, M. E. (2013). Keck II observations of hemispherical differences in H₂O₂ on Europa. *The Astrophysical Journal Letters*, 766(2), L21. <https://doi.org/10.1088/2041-8205/766/2/L21>
- Hartogh, P., Jarchow, C., Lellouch, E., de Val-Borro, M., Rengel, M., Moreno, R., et al. (2010). Herschel/HIFI observations of Mars: First detection of O₂ at submillimeter wavelengths and upper limits on HCl and H₂O₂. *Astronomy & Astrophysics*, 521, L49. <https://doi.org/10.1051/0004-6361/201015160>
- Holmes, J. A., Lewis, S. R., & Patel, M. R. (2017). On the link between Martian total ozone and potential vorticity. *Icarus*, 282, 104–117. <https://doi.org/10.1016/j.icarus.2016.10.004>
- Holmes, J. A., Lewis, S. R., Patel, M. R., & Lefèvre, F. (2018). A reanalysis of ozone on Mars from assimilation of SPICAM observations. *Icarus*, 302, 308–318. <https://doi.org/10.1016/j.icarus.2017.11.026>
- Khayat, A. S. J., Smith, M. D., Wolff, M., Daerden, F., Neary, L., Patel, M. R., et al. (2021). ExoMars TGO/NOMAD-UVIS vertical profiles of ozone: 2. The high-altitude layers of atmospheric ozone. *Journal of Geophysical Research: Planets*, 126(11), e2021JE006834. <https://doi.org/10.1029/2021JE006834>
- Khayat, A. S. J., Smith, M. D., Wolff, M. J., Guzewich, S. D., Mason, E. L., & Atwood, S. A. (2023). The Mars atmosphere water ice aerosol climatology by MRO/CRISM: 5 Mars years of observations. *Journal of Geophysical Research: Planets*, 128(7), e2023JE007761. <https://doi.org/10.1029/2023JE007761>
- Kim, H. C., Lee, P., Ngan, F., Tang, Y., Yoo, H. L., & Pan, L. (2015). Evaluation of modeled surface ozone biases as a function of cloud cover fraction. *Geoscientific Model Development*, 8(9), 2959–2965. <https://doi.org/10.5194/gmd-8-2959-2015>
- Kolb, C. E., Cox, R. A., Abbatt, J. P. D., Ammann, M., Davis, E. J., Donaldson, D. J., et al. (2010). An overview of current issues in the uptake of atmospheric trace gases by aerosols and clouds. *Atmospheric Chemistry and Physics*, 10(21), 10561–10605. <https://doi.org/10.5194/acp-10-10561-2010>
- Kong, T. Y., & McElroy, M. B. (1977). The global distribution of O₃ on Mars. *Planetary and Space Science*, 25(9), 839–857. [https://doi.org/10.1016/0032-0633\(77\)90038-1](https://doi.org/10.1016/0032-0633(77)90038-1)
- Korablev, O., Olsen, K. S., Trokhimovskiy, A., Lefèvre, F., Montmessin, F., Fedorova, A. A., et al. (2021). Transient HCl in the atmosphere of Mars. *Science Advances*, 7(7), eabe4386. <https://doi.org/10.1126/sciadv.abe4386>
- Korablev, O., Vandaele, A. C., Montmessin, F., Fedorova, A. A., Trokhimovskiy, A., Forget, F., et al. (2019). No detection of methane on Mars from early ExoMars trace gas orbiter observations. *Nature*, 568(7753), 517–520. <https://doi.org/10.1038/s41586-019-1096-4>
- Korablev, O. I., Montmessin, F., Trokhimovskiy, A., Fedorova, A. A., Shakun, A. V., Grigoriev, A. V., et al. (2018). The atmospheric chemistry suite (ACS) of three spectrometers for the ExoMars 2016 trace gas orbiter. *Space Science Reviews*, 214(1), 7. <https://doi.org/10.1007/s11214-017-0437-6>
- Krasnopolsky, V. A. (1986). *Photochemistry of the atmospheres of Mars and Venus*. Springer.
- Krasnopolsky, V. A. (1993). Photochemistry of the Martian atmosphere (mean conditions). *Icarus*, 101(2), 313–332. <https://doi.org/10.1006/icar.1993.1027>
- Krasnopolsky, V. A. (2006). Photochemistry of the Martian atmosphere: Seasonal, latitudinal, and diurnal variations. *Icarus*, 185(1), 153–170. <https://doi.org/10.1016/j.icarus.2006.06.003>
- Krasnopolsky, V. A. (2009). Seasonal variations of photochemical tracers at low and middle latitudes on Mars: Observations and models. *Icarus*, 201(2), 564–569. <https://doi.org/10.1016/j.icarus.2009.01.017>

- Krasnopolsky, V. A., Bjoraker, G. L., Mumma, M. J., & Jennings, D. E. (1997). High-resolution spectroscopy of Mars at 3.7 and 8 μm : A sensitive search for H_2O_2 , H_2CO , HCl , and CH_4 , and detection of HDO . *Journal of Geophysical Research*, *102*(E3), 6525–6534. <https://doi.org/10.1029/96je03766>
- Kuroda, T., Medvedev, A. S., Kasaba, Y., & Hartogh, P. (2013). Carbon dioxide ice clouds, snowfalls, and baroclinic waves in the northern winter polar atmosphere of Mars. *Geophysical Research Letters*, *40*(8), 1484–1488. <https://doi.org/10.1002/grl.50326>
- Lamarque, J.-F., McConnell, J. R., Shindell, D. T., Orlando, J. J., & Tyndall, G. S. (2011). Understanding the drivers for the 20th century change of hydrogen peroxide in Antarctic ice-cores. *Geophysical Research Letters*, *38*(4), L04810. <https://doi.org/10.1029/2010GL045992>
- Lebonnois, S., Quémerais, E., Montmessin, F., Lefèvre, F., Perrier, S., Bertaux, J.-L., & Forget, F. (2006). Vertical distribution of ozone on Mars as measured by SPICAM/Mars Express using stellar occultations. *Journal of Geophysical Research*, *111*(E9), E09S05. <https://doi.org/10.1029/2005JE002643>
- Lefèvre, F., Bertaux, J.-L., Clancy, R. T., Encrenaz, T., Fast, K., Forget, F., et al. (2008). Heterogeneous chemistry in the atmosphere of Mars. *Nature*, *454*(7207), 971–975. <https://doi.org/10.1038/nature07116>
- Lefèvre, F., & Krasnopolsky, V. (2017). Atmospheric photochemistry. In R. M. Haberle, R. T. Clancy, F. Forget, M. D. Smith, & R. W. Zurek (Eds.), *The atmosphere and climate of Mars* (pp. 405–432). Cambridge University Press.
- Lefèvre, F., Lebonnois, S., Montmessin, F., & Forget, F. (2004). Three-dimensional modeling of ozone on Mars. *Journal of Geophysical Research*, *109*(E7), E07004. <https://doi.org/10.1029/2004JE002268>
- Lefèvre, F., Trokhimovskiy, A., Fedorova, A., Baggio, L., Lacombe, G., Määttänen, A., et al. (2021). Relationship between the ozone and water vapour columns on Mars as observed by SPICAM and calculated by a global climate model. *Journal of Geophysical Research: Planets*, *126*(4), e2021JE006838. <https://doi.org/10.1029/2021JE006838>
- Lindner, B. L. (1988). Ozone on Mars: The effects of clouds and airborne dust. *Planetary and Space Science*, *36*(2), 125–144. [https://doi.org/10.1016/0032-0633\(88\)90049-9](https://doi.org/10.1016/0032-0633(88)90049-9)
- Loeffler, M. J., & Baragiola, R. A. (2005). The state of hydrogen peroxide on Europa. *Geophysical Research Letters*, *32*(17), 17202. <https://doi.org/10.1029/2005gl023569>
- Loeffler, M. J., & Baragiola, R. A. (2011). Isothermal decomposition of hydrogen peroxide dihydrate. *Journal of Physical Chemistry A*, *115*(21), 5324–5328. <https://doi.org/10.1021/jp200188b>
- Loeffler, M. J., Fama, M., Baragiola, R. A., & Carlson, R. W. (2013). Photolysis of H_2O – H_2O_2 mixtures: The destruction of H_2O_2 . *Icarus*, *226*(1), 945–950. <https://doi.org/10.1016/j.icarus.2013.06.030>
- Loeffler, M. J., Teolis, B. D., & Baragiola, R. A. (2006). Distillation kinetics of solid mixtures of hydrogen peroxide and water and the isolation of pure hydrogen peroxide in ultrahigh vacuum. *Journal of Physical Chemistry B*, *110*(13), 6911–6915. <https://doi.org/10.1021/jp060289s>
- Maass, O., & Hiebert, P. G. (1924). The properties of pure hydrogen peroxide. V. Vapor pressure. *Journal of the American Chemical Society*, *46*(12), 2693–2700. <https://doi.org/10.1021/ja01677a012>
- Määttänen, A., Lefèvre, F., Verdier, L., Montmessin, F., Listowski, C., Guilbon, S., et al. (2022). Ozone vertical distribution in Mars Years 27–30 from SPICAM/MEX UV occultations. *Icarus*, *387*, 115162. <https://doi.org/10.1016/j.icarus.2022.115162>
- Marti, J., & Mauersberger, K. (1993). A survey and new measurements of ice vapor pressure at temperatures between 170 and 250 K. *Geophysical Research Letters*, *20*(5), 363–366. <https://doi.org/10.1029/93GL00105>
- Mauersberger, K., & Krankowsky, D. (2003). Vapor pressure above ice at temperatures below 170 K. *Geophysical Research Letters*, *30*(3), 1121. <https://doi.org/10.1029/2002GL016183>
- McElroy, M. B., & Donahue, T. M. (1972). Stability of the Martian atmosphere. *Science*, *177*(4053), 986–988. <https://doi.org/10.1126/science.177.4053.986>
- Montabone, L., Forget, F., Millour, E., Wilson, R. J., Lewis, S. R., Cantor, B., et al. (2015). Eight-year climatology of dust optical depth on Mars. *Icarus*, *251*, 65–95. <https://doi.org/10.1016/j.icarus.2014.12.034>
- Montabone, L., Spiga, A., Kass, D. M., Kleinböhl, A., Forget, F., & Millour, E. (2019). Martian year 34 column dust climatology from Mars climate sounder observations: Reconstructed maps and model simulations. *Journal of Geophysical Research: Planets*, *125*(8), e2019JE006111. <https://doi.org/10.1029/2019JE006111>
- Montmessin, F., Korabev, O., Lefèvre, F., Bertaux, J.-L., Fedorova, A., Trokhimovskiy, A., et al. (2017). SPICAM on Mars express: A 10 year in-depth survey of the martian atmosphere. *Icarus*, *297*, 195–216. <https://doi.org/10.1016/j.icarus.2017.06.022>
- Montmessin, F., & Lefèvre, F. (2013). Transport-driven formation of a polar ozone layer on Mars. *Nature Geoscience*, *6*(11), 930–933. <https://doi.org/10.1038/ngeo1957>
- Moreau, D., Esposito, L. W., & Brasseur, G. (1991). The chemical composition of the dust-free Martian atmosphere: Preliminary results of a two-dimensional model. *Journal of Geophysical Research*, *96*(B5), 7933–7945. <https://doi.org/10.1029/90jb02544>
- Moudden, Y. (2007). Simulated seasonal variations of hydrogen peroxide in the atmosphere of Mars. *Planetary and Space Science*, *55*(14), 2137–2143. <https://doi.org/10.1016/j.pss.2007.06.005>
- Moudden, Y., & McConnell, J. C. (2007). Three-dimensional on-line chemical modeling in a Mars general circulation model. *Icarus*, *188*(1), 18–34. <https://doi.org/10.1016/j.icarus.2006.11.005>
- Murchie, S. (2006). MRO CRISM derived data record V1.0 [Dataset]. NASA Planetary Data System. <https://doi.org/10.17189/1519567>
- Murchie, S., Arvidson, R., Bedini, P., Beisser, K., Bibring, J.-P., Bishop, J., et al. (2007). Compact reconnaissance imaging spectrometer for Mars (CRISM) on Mars Reconnaissance orbiter (MRO). *Journal of Geophysical Research*, *112*(E5), E05S03. <https://doi.org/10.1029/2006JE002682>
- Navarro, T., Madeleine, J.-B., Forget, F., Spiga, A., Millour, E., Montmessin, F., & Määttänen, A. (2014). Global climate modeling of the Martian water cycle with improved microphysics and radiatively active water ice clouds. *Journal of Geophysical Research: Planets*, *119*(7), 1479–1495. <https://doi.org/10.1002/2013JE004550>
- Neary, L., & Daerden, F. (2018). The GEM-mars general circulation model for Mars: Description and evaluation. *Icarus*, *300*, 458–476. <https://doi.org/10.1016/j.icarus.2017.09.028>
- Neftel, A., Jacob, P., & Klockow, D. (1984). Measurements of hydrogen peroxide in polar ice samples. *Nature*, *311*(5981), 43–45. <https://doi.org/10.1038/311043a0>
- Neftel, A., Jacob, P., & Klockow, D. (1986). Long-term record of H_2O_2 in polar ice cores. *Tellus*, *388*(3–4), 262–270. <https://doi.org/10.1111/j.1600-0889.1986.tb00192.x>
- Nikolakakos, G., & Whiteway, J. A. (2015). Laboratory investigation of perchlorate deliquescence at the surface of Mars with a Raman scattering lidar. *Geophysical Research Letters*, *42*(19), 7899–7906. <https://doi.org/10.1002/2015GL065434>
- Nikolakakos, G., & Whiteway, J. A. (2018). Laboratory study of adsorption and deliquescence on the surface of Mars. *Icarus*, *308*, 221–229. <https://doi.org/10.1016/j.icarus.2017.05.006>
- Olsen, K. S., Lefèvre, F., Montmessin, F., Trokhimovskiy, A., Baggio, L., Fedorova, A., et al. (2020). First detection of ozone in the mid-infrared at Mars: Implications for methane detection. *Astronomy & Astrophysics*, *639*, A141. <https://doi.org/10.1051/0004-6361/202038125>

- Parkinson, T. D., & Hunten, D. M. (1972). Spectroscopy and aeronomy of O₂ on Mars. *Journal of the Atmospheric Sciences*, 29(7), 1380–1390. [https://doi.org/10.1175/1520-0469\(1972\)029<1380:saoooo>2.0.co;2](https://doi.org/10.1175/1520-0469(1972)029<1380:saoooo>2.0.co;2)
- Parks, M. C., Nixon, C. A., Villanueva, G. L., Smith, M. D., Khayat, A. S. J., Thelen, A. E., et al. (2021). Observations of Mars with ALMA: Potential for future constraints of global circulation models. *Journal of Astronomical Telescopes, Instruments, and Systems*, 7(2), 025001. <https://doi.org/10.1117/1.JATIS.7.2.025001>
- Patel, M. R., Sellers, G., Mason, J. P., Holmes, J. A., Brown, M. A. J., Lewis, S. R., et al. (2021). ExoMars TGO/NOMAD-UVIS vertical profiles of ozone: 1. Seasonal variation and comparison to water. *Journal of Geophysical Research: Planets*, 126(11), e2021JE006837. <https://doi.org/10.1029/2021JE006837>
- Perrier, S., Bertaux, J. L., Lefèvre, F., Lebonnois, S., Korabiev, O., Fedorova, A., & Montmessin, F. (2006). Global distribution of total ozone on Mars from SPICAM/MEX UV measurements. *Journal of Geophysical Research*, 111(E9), E09S06. <https://doi.org/10.1029/2006JE002681>
- Picaud, S., & Jedlovsky, P. (2014). Adsorption of H₂O₂ at the surface of I_h ice, as seen from grand canonical Monte Carlo simulations. *Chemical Physics Letters*, 600, 73–78. <https://doi.org/10.1016/j.cplett.2014.03.050>
- Piccialli, A., Vandaele, A. C., Willame, Y., Määttänen, A., Trompet, L., Erwin, J. T., et al. (2023). Martian ozone observed by TGO/NOMAD-UVIS solar occultation: An inter-comparison of three retrieval methods. *Earth and Space Science*, 10(2), e2022EA002429. <https://doi.org/10.1029/2022EA002429>
- Pouvesle, N., Kippenberger, M., Schuster, G., & Crowley, J. N. (2010). The interaction of H₂O₂ with ice surfaces between 203 and 233 K. *Physical Chemistry Chemical Physics*, 12(47), 15544–15550. <https://doi.org/10.1039/c0cp01656j>
- Rivera-Valentín, E. G., Chevrier, V. F., Soto, A., & Martínez, G. (2020). Distribution and habitability of (meta)stable brines on present-day Mars. *Nature Astronomy*, 4(8), 756–761. <https://doi.org/10.1038/s41550-020-1080-9>
- Robert, S., Vandaele, A. C., Thomas, I., Willame, Y., Daerden, F., Delanoye, S., et al. (2016). Expected performances of the NOMAD/ExoMars instrument. *Planetary and Space Science*, 124, 94–104. <https://doi.org/10.1016/j.pss.2016.03.003>
- Ryu, Y.-H., Hodzic, A., Descombes, G., Hall, S., Minnis, P., Spangenberg, D., et al. (2017). Improved modeling of cloudy-sky actinic flux using satellite cloud retrievals. *Geophysical Research Letters*, 44(3), 1592–1600. <https://doi.org/10.1002/2016GL071892>
- Schumb, W. C., Satterfield, C. N., & Wentworth, R. L. (1955). *Hydrogen peroxide*. Reinhold.
- Sigg, A., & Neftel, A. (1988). Seasonal variations in hydrogen peroxide in polar ice cores. *Annals of Glaciology*, 10, 157–162. <https://doi.org/10.1017/s0260305500004353>
- Smith, M., Daerden, F., Neary, L., & Khayat, A. (2018). The climatology of carbon monoxide and water vapour on Mars as observed by CRISM and modeled by the GEM-Mars general circulation model. *Icarus*, 301, 117–131. <https://doi.org/10.1016/j.icarus.2017.09.027>
- Solomon, S. (1999). Stratospheric ozone depletion: A review of concepts and history. *Reviews of Geophysics*, 37(3), 275–316. <https://doi.org/10.1029/1999rg900008>
- Trumbo, S. K., Brown, M. E., Bockelée-Morvan, D., de Pater, I., Fouchet, T., Wong, M. H., et al. (2023). Hydrogen peroxide at the poles of Ganymede. *Science Advances*, 9(29), eadg3724. <https://doi.org/10.1126/sciadv.adg3724>
- Vandaele, A. C., Korabiev, O., Daerden, F., Aoki, S., Thomas, I. R., Altieri, F., et al. (2019). Martian dust storm impact on atmospheric H₂O and D/H observed by ExoMars Trace Gas Orbiter. *Nature*, 568(7753), 521–525. <https://doi.org/10.1038/s41586-019-1097-3>
- Vandaele, A. C., Lopez-Moreno, J.-J., Patel, M. R., Bellucci, G., Daerden, F., Ristic, B., et al. (2018). NOMAD, an integrated suite of three spectrometers for the ExoMars trace gas mission: Technical description, science objectives and expected performance. *Space Science Reviews*, 214(5), 80. <https://doi.org/10.1007/s11214-018-0517-2>
- Villanueva, G. L., Mumma, M. J., Novak, R. E., Radeva, Y. L., Käufel, H. U., Smette, A., et al. (2013). A sensitive search for organics (CH₄, CH₃OH, H₂CO, C₂H₆, C₂H₂, C₂H₄), hydroperoxyl (HO₂), nitrogen compounds (N₂O, NH₃, HCN) and chlorine species (HCl, CH₃Cl) on Mars using ground-based high-resolution infrared spectroscopy. *Icarus*, 223(1), 11–27. <https://doi.org/10.1016/j.icarus.2012.11.013>
- Willame, Y., Vandaele, A. C., Depiesse, C., Lefèvre, F., Letocart, V., Gillotay, D., & Montmessin, F. (2017). Retrieving cloud, dust and ozone abundances in the Martian atmosphere using SPICAM/UV nadir spectra. *Planetary and Space Science*, 142, 9–25. <https://doi.org/10.1016/j.pss.2017.04.011>
- Wolff, M. J., Clancy, R. T., Kahre, M. A., Haberle, R. M., Forget, F., Cantor, B. A., & Malin, M. C. (2019). Mapping water ice clouds on Mars with MRO/MARCI. *Icarus*, 332, 24–49. <https://doi.org/10.1016/j.icarus.2019.05.041>
- Zurek, R. W., Chicarro, A., Allen, M. A., Bertaux, J.-L., Clancy, R. T., Daerden, F., et al. (2011). Assessment of a 2016 mission concept: The search for trace gases in the atmosphere of Mars. *Planetary and Space Science*, 59(2–3), 284–291. <https://doi.org/10.1016/j.pss.2010.07.007>
- Zurek, R. W., & Smrekar, S. E. (2007). An overview of the Mars Reconnaissance Orbiter (MRO) science mission. *Journal of Geophysical Research*, 112(E5), E05S01. <https://doi.org/10.1029/2006JE002701>

References From the Supporting Information

- Appéré, T., Schmitt, B., Langevin, Y., Douté, S., Pommerol, A., Forget, F., et al. (2011). Winter and spring evolution of northern seasonal deposits on Mars from OMEGA on Mars Express. *Journal of Geophysical Research*, 116(E5), E05001. <https://doi.org/10.1029/2010JE003762>
- Hébrard, E., Listowski, C., Coll, P., Marticorena, B., Bergametti, G., Määttänen, A., et al. (2012). An aerodynamic roughness length map derived from extended Martian rock abundance data. *Journal of Geophysical Research*, 117(E4), E04008. <https://doi.org/10.1029/2011JE003942>
- Kreslavsky, M. A., & Head, J. W., III. (2000). Kilometer scale roughness on Mars: Results from MOLA data analysis. *Journal of Geophysical Research*, 105(E11), 26695–26711. <https://doi.org/10.1029/2000je001259>
- Orosei, R., Bianchi, R., Coradini, A., Espinasse, S., Federico, C., Ferriccioni, A., & Gavrishin, A. I. (2003). Self-affine behavior of Martian topography at kilometer scale from Mars orbiter laser altimeter data. *Journal of Geophysical Research*, 108(E4), 8023. <https://doi.org/10.1029/2002JE001883>
- Pardo-Igúzquiza, E., & Dowd, P. A. (2022). Fractal analysis of the Martian landscape: A study of kilometer-scale topographic roughness. *Icarus*, 372, 114727. <https://doi.org/10.1016/j.icarus.2021.114727>
- Savijärvi, H. I., & Harri, A.-M. (2021). Water vapor adsorption on Mars. *Icarus*, 357, 114270. <https://doi.org/10.1016/j.icarus.2020.114270>
- Smith, M. D. (2004). Interannual variability in TES atmospheric observations of Mars during 1999–2003. *Icarus*, 167(1), 148–165. <https://doi.org/10.1016/j.icarus.2003.09.010>